Modeling of a Dielectric Elastomer

Mesfer Alkhathami

A Thesis

in

The Department

of

Mechanical, Industrial and Aerospace Engineering

Presented in Partial Fulfillment of the Requirements

for the Degree of

Master of Applied Science (Mechanical Engineering) at

Concordia University

Montréal, Québec, Canada

October 2018

CONCORDIA UNIVERSITY

School of Graduate Studies

This is to certify that the thesis prepared

By: **Mesfer Alkhathami**

Entitled: **Modeling of a Dielectric Elastomer**

and submitted in partial fulfillment of the requirements for the degree of

Master of Applied Science (Mechanical Engineering)

complies with the regulations of this University and meets the accepted standards with respect to originality and quality.

Signed by the Final Examining Committee:

_____ Chair
Dr. Mingyuan Chen

_____ External Examiner
Dr. Lan Lin

_____ Examiner
Dr. Youmin Zhang

_____ Supervisor
Dr. Chun-Yi Su

Approved by _____
Martin D. Pugh, Chair
Department of Mechanical, Industrial and Aerospace Engineering

_____ 2018

_____
Amir Asif, Dean
Faculty of Engineering and Computer Science

Abstract

Modeling of a Dielectric Elastomer

Mesfer Alkhathami

Dielectric elastomer actuator (DEA) is a key element for the soft robots, which has received increasing attention. However, the main difficulties in modeling soft actuators such as dielectric elastomer actuators are time-dependent viscoelasticity and their material nonlinearity. It is important to consider the viscoelasticity of the dielectric elastomer (DE) to fully understand its mechanical behavior. However, so far only a few works have been presented considering the viscoelasticity of the DE material together with the effect of temperature and deformation.

In this thesis, a dynamic electromechanical-coupled model for a rectangle dielectric elastomer a commonly used material (the acrylic elastomer VHB 4910) has been proposed, with taking into consideration of the influence of temperature, voltage, and frequency on the DE. The proposed model is based on the free energy physical-based principle, where the general Kelvin-Voigt model is applied to describe the viscoelasticity of the DE, and the Maxwell force together with the Electrostrictive force are considered. The influence of temperature and deformation on the DE is included in this model. The model in this study is a dynamic electromechanical model of a DE actuator, and can effectively describe the dynamic characteristics of the DE.

By using the Differential Evolution, the model parameters were identified. The model was implemented and simulated in MATLAB, and the simulation and the actual experiment agrees to a great extent. The experimental test conducted in this study matches with the simulations results, which means that the proposed model can be practical to predict and describe DEAs electromechanical and viscoelastic behavior. Predicting the electromechanical and viscoelastic behavior of the DE is extremely useful for controlling a viscoelastic DEA and paving the way to improve the control performance, and also develops applications in soft robotics.

Acknowledgments

I would like to thank my supervisor, Dr. Chun-Yi Su, for constant guidance, and for supporting my ideas through my Master studies.

A very special thanks goes to my friend Dr. Yawu Wang who have inspired me with his great ideas concerning the modeling of Dielectric Elastomer actuators, constantly supported me with experimental tests, and have made my experience unforgettable one.

I personally thank my colleagues for their constant support and my friends Dr. Yilong Zhang and Dr. Wenjun Ye for their generous advices and support.

Last but not least, I would like to thank my family for their support.

Contents

List of Figures

List of Tables

Chapter 1

Introduction

1.1 Objective of the Thesis

In robotics society, DEAs have attracted the research attention and have shown promise for the applications of the soft robotics field due to their interesting combination of properties, including large deformation, high energy density, low cost, lightweight, good efficiency, and fast response. However, the DEs materials exhibit high nonlinear viscoelasticity, hysteresis, creep, and vibrational dynamics, which makes modeling it a challenging task to do. The dielectric elastomers are highly nonlinear materials, which makes its dynamic behavior complex when stretching, and experience creep under constant loads, and hysteresis upon cyclic loading. Thus, the mechanical responses of DEAs are strong nonlinear, time-dependent and frequency dependent.

Numerous investigations have focused on static or quasi-static applications. A few works reported the effect of inertia and viscoelasticity in DEs together with the influence of temperature and deformation. Recently, researchers have investigated the dynamic behavior of the DE membrane to have better understanding on how the DE behaves. Nevertheless, the dynamic behavior of DEAs needs to be studied in details and its inherent nonlinear effects demand new control concepts. In addition, many studies have claimed that temperature has an impact on the performance of the DE.

In this study, a dynamic model of the most widely used material VHB 4910 is proposed with accounting for the viscoelasticity of DEAs (specifically the creep), temperature dependent, voltages, and frequencies. The simulations of the model are provided with different voltages, frequencies,

and temperatures. Moreover, experimental tests are applied, and the simulations results and experimental results show the validity of the presented model.

1.2 Orgnization of the Thesis

This thesis consists of 5 chapters including the introduction in Chapter 1. The topics of the rest chapters are organized as follows:

- **Chapter 2:**

  A literature review of dielectric elastomer is presented including electromechanical modeling approaches and reviews of the soft robots using dielectric elastomer actuators.

- **Chapter 3:**

  A detailed modeling of a DE with rectangle shape is proposed.

- **Chapter 4:**

  The proposed DE model will be simulated, and the effectiveness of the model will be validated by the experiment test. Also, the experimental setup is introduced with materials used followed by a discussion on the phenomena observed in experiments. The theoretical and experimental comparisons are discussed as well in this chapter.

- **Chapter 5:**

  Conclusions and future works will be included.

Chapter 2

Literature Review

2.1 Dielectric Elastomer

In artificial muscle technology, the use of soft elastomers such as silicones, acrylics and polyurethanes have been studied extensively (Rosset & Shea, 2013). Electro-Active Polymers (EAPs) represent an innovative class of smart materials, which exhibit a change in size or shape when subjected to an external electrical stimuli (Maffli, Rosset, & Shea, 2013). Dielectric EAPs (DEAPs), most commonly referred to as Dielectric Elastomers (DEs), represent a class of electronic EAPs consisting of a film of elastic polymeric material covered on both sides by compliant electrodes. This kind of EAPs, known as electronic EAPs, requires high driving voltages, possess high electrical energy and can be operated in the air. When a voltage is applied to the electrodes, the resulting electric field generates a compressive stress that produces a controllable deformation (Rosset & Shea, 2013).

As a comparison to other smart materials (e.g., piezoelectric ceramics, shape memory alloys), the deformation of DEs can be in some cases one or two orders of magnitude larger. Large deformation (¿100% in many cases), high actuation speeds, high work densities and a high degree of electromechanical coupling make dielectric elastomers are the most favorable in actuation, and an attractive alternative for the development of a new generation of mechatronic devices (Rosset & Shea, 2013). In fact, several prototypes of DEs applications have been presented, such as pumps (Rosset & Shea, 2013), valves (Giousouf & Kovacs, 2013), loudspeakers (Sugimoto et al., 2013),

robots (R. Pelrine et al., 2002) (Pei, Rosenthal, Stanford, Prahlad, & Pelrine, 2004) (Godaba, Li, Wang, & Zhu, 2016), flap- ping wing insects (Heydt, Kornbluh, Eckerle, & Pelrine, 2006), optical positioning systems (Son et al., 2012), micro-positioning stages (Jordan et al., 2011), pressure or deformation sensors (Iskandarani & Karimi, 2012), and energy harvesters (Vertechy, Fontana, Papini, & Bergamasco, 2013).

Researchers have made a significant development in the use of DEAs in the past decades, especially in the field of materials and physics, and a great number of robots have been designed and developed using DEAs materials. However, there are many technological issues that still need to be properly addressed in order to make this material competitive in industrial applications. For instance, the amount of voltage needed to obtain a significant deformation, the strong nonlinearities in the input-output characteristics, and the dependence of the response on environmental conditions and fatigue.

2.1.1 Soft Robotics

Over the last decade, soft robotics have been a promising field of research and a variety of soft robots have been enhanced using different actuation technologies and mechanisms (DuRant & You, 2014) (Marvel, Falco, & Marstio, 2015). Recently, soft robotics are technologically developed into two general areas, which are bio-inspired and bio-mimetic. The exponential grown of soft robotics technologies have led to more advanced developments in soft and smart materials, robotics mechanisms, and non-linear modelling due to countless benifits such as the ability of large deformation and the wide range of degree-of-freedoms. Taking into consideration the distinctness of actuation technologies, soft robots can be classified into two main groups (DuRant & You, 2014).

The first group is commonly known as continuum robots. This kind of soft robots is related to the tendon-driven actuation, and unlike traditional robots, they can be smoothly bent and continuously curving anywhere along their structure instead of bending at discrete points (joints, or elbows) (Robinson & Davies, 1999). Based on the type of the tendon-driven mechanisms (TDMs) with either intrinsicextrinsic hybrid actuators, extrinsic actuators, or intrinsic actuators the design of continuum robots could be rubber-like with unlimited degrees of freedom (DOFs). There are

many practical applications of this kind of robots, from medical and search to rescue applications. Nevertheless, few challenges have been identified of using continuum robots in the field of soft robotics. Generally, continuum robots deal with solid bodies not soft bodies. For example, one of their function is exploiting automatic transmission of the traditional motors and mechanisms such as ball screws and gears, which they are hard bodies.

The second group is in reference to the soft smart materials actuation. The characteristics of smart materials, named also as intelligent or responsive materials, make them changed as a result of the changes in their environment. They have the ability to significantly change from physical stimuli; for example, force, chemical, thermal, electric or magnetic sign to a physical displacement, unlike the tendon-driven actuation with the regular motors and transmission techniques. There are many areas which soft materials can be used in the field of soft robots such as Piezoelectrics, shape memory polymers (SMPs), the shape memory alloys (SMAs), Bi-Component Fibers, hydrogels and electro-active polymers (EAPs) (Rus & Tolley, 2015). SMPs and SMAs are type of materials that have the feature of undergoing large strain when they undergoing heating process (Majidi, 2014). In (Mazzolai, Margheri, Cianchetti, Dario, & Laschi, 2012), soft octopus arms were presented; however, it is difficult to precisely control SMAs due to its temperature dependent nature.

EAPs are a growing interest among researchers for years because of their unique factors and interesting advantages in many applications. EAPs, commonly referred to as artificial muscles, are attractive materials for the use in soft actuation technology, and that could be attributed to their flexibility and ability to change sizes and/or forms when an external condition is applied, such as an electric field or a voltage, and imitate the features of biological muscles (Laschi & Cianchetti, 2014). Examples of EAPs are dielectric EAPs, liquid crystal polymers, electrostrictive graft polymers, ferroelectric polymers, electrorheological fluids, stimuli-responsive gels, ionic polymermetal composites, and ionic EAPs. The use of EAPs are not limited in soft robotics, but they can also be used as pumps (Heim, Polyakov, Zarrabi, & Hui, 2009), valves (Jhong, Huang, Hsieh, & Fu, 2007), speakers (Heydt et al., 2006), and lens element actuators (H. Kim et al., 2007).

EAPs have different stimuli methods; by taking into account these differences, soft EAPs can be generally divided into two principal categories: electronic EAPs and ionic EAPs. Dielectric elastomers (DEs), which are the king of the electronic EAPs have some advantageous such as high

energy and power density, high efficiency, fast response speed, and inherent soft nature (Shepherd et al., 2011), which make them extremely beneficial in soft robotics. In contrast, ionic EAPs' coupling efficiency is poor and their actuation speeds are relatively slow (Mazzolai et al., 2012), which may limit their usefulness in the field of soft robotics. As an alternative option, it is worth mentioning that semi-active actuation suchlike electro-rheological foam/elastomers have been used for enhancing soft robots (Majidi, 2014). In this paper, rheological modeling is being used in this study to describe the viscoelasticity of the DE.

2.1.2 DEs Applications

The field of soft robotics shows good promising and opens a wide range of opportunities for the use of DEAs due to its unique performance. The DEAs show very promising performance as artificial muscles due to their high flexibility, lightweight and other factors compared with traditional rigid actuators DEA. The DEAs have been used in many kind of soft robots such as humanoid robots, swimming robots, serpentine robots, and flying robots.

Humanoid robots:

Prosthetic applications exhibit increasing attention, especially in the use of DEAs; readers may refer to (Biddiss & Chau, 2008) (Carpi, Frediani, & De Rossi, 2011) for overview of the obstacles and opportunities using DEAs for prosthetics. Virginia Tech presented a robotic arm, and in around four minutes it lifted a weight of 0.9 N and a height of 22 cm. According to the baseline human measurements, its speed capacity and force are lower than 1% (Biddiss & Chau, 2008). Carpi et al (Carpi, Frediani, & De Rossi, 2011) use DEAs to design a wearable device with tactile display, and in cyberspace a user can get a feedback during electronic navigation. Based on dielectric elastomer actuator Sensors, Lee et al presented an arrayed tactile display (Lee et al., 2014). It is designed to guarantee the safety of operation for the users while contacting with the human skin as well as adding the comfort of touch. In addition, the scientists have attempted to benefit from the astonishing properties of DEAs to simulate the eyeball muscle system of humans. Carpi and De Rossi (Carpi & De Rossi, 2005) presented bioinspired pseudo muscular eyeballs using DEAs for a humanoid robotic face.

Swimming robots:

In the growing interest in development of biomimetic and bioinspired swimming robots, the DEAs are one of the best options to choose due to their unique density that is approximately the same as that of water. In (Godaba et al., 2016), a DEA-based jellyfish robot was developed. Godabas experimental results show that the weight of the jellyfish robot is $256g$, and it has the ability to carry a payload of $236g$ compared to its actual-weight. Also, its maximum velocity was approximately 0.3 body length per second.

Walking/ serpentine robots:

A walking robot with DEA was the first kind of driven by biomimetic presented by Eckerle et al (Eckerle et al., 2001) in 2001; it was designed with six legs, and it was named as FLEX. Eckerle et al improved FLEX in 2002 by having more powerful rolled DEAs. MERbot is a DEA-driven walking robot with one 2-DOF-spring roll as each of its six legs, and it was demonstrated by Pei et al (Pei et al., 2004). Its speed is two-thirds of its length per second or as high as 13.6 cm s^1.

Flying robots:

DEAs produce a combination of large strain with high speed and energy density, and that make them a good choice for a potential actuation technology. In Singapore, a group of researchers at Nanyang Technological University (NTU) developed a bioinspired flapping wing robot with a lightweight carbon fiber reinforced polymer (CFRP) shell and rolled DEAs (Lau, Lim, Teo, & Chin, 2014). Furthermore, Shea s group from EPFL, Switzerland (Shintake, Rosset, Schubert, Floreano, & Shea, 2015), presented a foldable antagonistic actuator based on dielectric elastomers. The actuator can manage flight surfaces of a fixed wing drone with the angular displacement range and the torque condition of a $400mm$ wingspan micro-air vehicle of mass $130g$.

2.1.3 DEs Materials

The materials characteristics in the dielectric elastomer research should have some features such as high level of dielectric constant and breakdown strength, extremely low level of viscosity and electrical conductivity combined with a wide-ranging elastic moduli (Bauer et al., 2014). Researchers have investigated many kinds of elastomeric materials in the last decades. However,

polyurethanes (PUs), silicones and acrylics are the most frequently used elastomers, which they will be addressed in the following.

PUs:

In general, PUs have higher dielectric constant and relatively large output force, which make DEAs made of PU material require low electric fields to be actuated. Polyurethane elastomers are a part of segmented block copolymers that can be effectively used in biomedical applications (Lamba, 2017). However, the disadvantage of DEAs using PUs is the limitation of small strain, which makzes researchers pay no more attention to it.

Silicones:

Dielectric silicones elastomers are semi-inorganic polymers that are composed of a siloxane (Si-O) backbone. Dielectric elastomer actuators made of silicone elastomers show modest actuation strain, which is smaller than acrylics dielectric elastomers actuators, but larger than PUs dielectric elastomer actuators. As stated by (Brochu & Pei, 2010), DEAs with silicone elastomers operate at lower losses and higher frequencies. In addition, the silicone elastomers' electromechanical respond is fast (3s) with good reproducibility. Since silicones have a relatively low dielectric constant, they require higher electric fields for large strains (DuRant & You, 2014). However, silicones elastomers exhibit lower viscoelasticity, which is be considered as an advantage.

Acrylic:

Recently, soft elastomers have gained much attention in many industrial fields and research areas. Acrylic DEAs is the mostly and commonly used, particularly in the field of soft actuator technology. According to the study by Pelrine and colleagues (R. E. Pelrine, Kornbluh, & Joseph, 1998) (R. Pelrine, Kornbluh, Pei, & Joseph, 2000), acrylics are reported to be successfully choice for the large-strain DEAs. VHB acrylic elastomers from 3M have shown good performance by generating a large strain, a temperature dependency and a strong frequency (Godaba et al., 2016). The cost of VHB acrylic elastomer is commercially low and available (such as the most used VHB 4905 and VHB 4910), which is one of the reasons of its popularity.

The acrylic material produced by 3M Company is commonly used in soft robotics due to its magnificent strain property. For example, in the recent past, there are a large number of studies

reporting that the maximal area stretch of the 4910 type acrylic DE can be up to 380% after pre-stretching. Moreover, DEAs using the prestretched 3M VHB acrylic elastomer can produce area strains more than 1000% (Godaba, Foo, Zhang, Khoo, & Zhu, 2014) as well as giant voltage-induced linear strains over 380% (Zhao, 2014). However, the strong viscoelastic nonlinearities that acrylics experience (Hong, 2011) (Chiang Foo, Cai, Jin Adrian Koh, Bauer, & Suo, 2012) could adversely affect the performance of a dielectric elastomer actuator and limits its applications.

2.2 Advantages and Dis Advantages of DE

2.2.1 Advantages of DEs

Dielectric elastomers are smart materials as they change their shape under the influence of electric field. DEAs have shown their usefulness in soft robotics field for their unique materials properties. When electric field is applied, DEs can produce high energy density approximate ($> 3.4MJm^{-3}$) and large deformation up to ($> 100\%$). What is more, it possesses the advantages of high elastic energy density, fast responses (in millisecond), high electromechanical conversion rate, excellent flexibility, lightweight (approximately as that of water), and low cost. The main attractive advantages that make dielectric elastomers extremely beneficial, especially in soft robotics applications, is the ability to generate resemble natural muscle of humans, and mimic the muscles in our human bodies with regard to producing large actuation strain (displacement per length unit) and actuating density and force compared to other competitors (Shepherd et al., 2011).

Koh et al. (Koh et al., 2011) achieved actuation strains of up to 1692%, and also a theoretical maximum energy density of $1.4J/g$ has been reached (Keplinger, Kaltenbrunner, Arnold, & Bauer, 2010). DEAs, popularly referred to as artificial muscles, represent a promising alternative to existing conventional engineering mechanisms. DEAs can enable new kinds of robotics, and greatly expand the engineering design space. There is a wide range of applications and devices that can be created by the use of DEAs such as a fish-like blimp and a linear actuator.

2.2.2 Disdvantages of DEs

Non-linear viscoelasticity:

A common disadvantage for DEs, especially the most widely used VHB 4910, is that the dielectric elastomer exhibits a high nonlinear viscoelasticity. The dissipative behaviour such as the Mullins effect, frequency dependent response, hysteresis, and creep affect the performance and limit the application of DE-based mechanisms (Gu, Zhu, Zhu, & Zhu, 2017).

Temperature Dependency:

The DE materials, especially Acrylic type, are temperature dependent, and the temperature affects the performance of the DEs. For example, the electromechanical deformation of dielectric elastomers is influended by the temperature, which makes the temperature an important factor when it come to modeling the DEAs. However, it is a challenging task to consider the temperature factor in modeling the DEs since the temperature dependency is high for DEs materials (Michel, Zhang, Wissler, Löwe, & Kovacs, 2010) (Sahu, Patra, & Szpunar, 2015) (Patra & Sahu, 2015) (L. Liu et al., 2015).

Safety:

DEAs are Electrically capacitors that can be actuated by storing electrical energy on their electrodes, and electrical safety could be one of the main issues about the DEAs. Generally, DEAs use high direct current (DC) and alternating current (AC) voltages (mostly higher than 1 kV) to be activated, and storing charges poses a serious danger to the user if discharged to the body. Therefore, ensuring electrical safety is extremely important, and requires a proper design of DEAs. However, DEAs need a small current in general (on the order of 10^{-6}A), and by limiting the current and energy level these concerns can be eliminated (Gu et al., 2017).

2.3 Modeling Approach

2.3.1 Electromechanical Modeling Approaches

Pelrine and colleagues presented the first physical-based model to represent the electromechanical characteristics of dielectric elastomer actuators (R. Pelrine et al., 2000). The electrostatic pressure from one electrode's side of DEAs to the other can be described by the resulting electrostatic stress when a prestreched DEA is subjected to a voltage V, and it is defined by the sum of the material's permittivity multiplied by the square root of the electric field applied E as expressed below:

$$P = \varepsilon_0 \varepsilon_r * E^2 \tag{1}$$

where P refers to Maxwell stress, which is the compressive effective stress, ε_0 is absolute permittivity (its value is approximately $8.85 * 10^{-12} Fm^{-1}$) and ε_r is the relative permittivity of dielectric elastomers. In equation (1), the effective compressive stress is double the stress usually used for two charged capacitor plates because the planar stretching in DEAs is attached to the thickness compression. In equation (1), the dielectric elastomer is taken to be ideal, so the Maxwell stress is a result from tensile stresses acting in the planar direction as well as the compressive stress acting in the thickness direction. Based on equation (1), in a light layer to a single compressive stress acting in the thickness direction, the tensile and compressive stresses are mechanically equivalent.

It is been widely known that the dielectric behavior of the elastomer is considered to be liquid-like and uninfluenced by deformation, and this model is used effectively to express the DEAs' electromechanical behavior (Carpi, De Rossi, Kornbluh, Pelrine, & Sommer-Larsen, 2011) (Keplinger et al., 2010) (Rizzello, Naso, York, & Seelecke, 2015). For low strains (e.g., $< 20\%$), thickness strain s_z is approximated as:

$$s_z = -p/Y = -\varepsilon_0 \varepsilon_1 * E^2/Y \tag{2}$$

Y is being the elastic modulus relating to the strain. Since Y is dependent on the strain itself on most cases, this function failed for strains greater than 20%. The electromechanical energy density can be applied to measure the performance of nonlinear materials under high strain where the compressive

stress is known, and the expression of the electromechanical energy density is as follows:

$$e = -pln(1 + S_z) \tag{3}$$

where p is the constant compressive stress. In terms of high strain, the density of electromechanical energy can estimate the the thickness strain s_z, given by

$$s_z = e^{-w_e/p} - 1 \tag{4}$$

w_e is the density of electromechanical energy, denoted as the change amount of electrical charges to mechanical energy per unit volume of the DEAs for one cycle. Since we assume that the dielectric elastomer is ideal, eq.(2) or (4) can obtain the strains on the plane based on thickness strain. As shown in (1), the stress is proportional to the permittivity of the dielectric elastomers while it is inversely proportional to the thickness of the elastomer membrane. For this reason, the thickness of the membrane decreases as the electric field across the thickness increases when a DEA is subjected to a voltage.

The changing of thickness in DEs results in electromechanical instability or electrical breakdown as well as limiting strain performance of DEAs, which can affect its functioning. The actuation of DEAs can also be negatively affected by the inherent nonlinearity that dielectric elastomers exhibit, which is defined as viscoelasticity. Even though Pelrines approach described in (1)-(4) simplify the understanding of electrical behaviour of DEAs, it cannot successfully take into consideration nonlinear elasticity and the large-deformed nonlinearity of DEAs.

2.3.1.1 Energy-based Electromechanical Modeling

For predicting the nonlinear elastic behaviors and the large-deformation nonlinearity of rubber-like materials, especially in DEAs, Energy-based analytical approaches are effectively useful (Kofod, 2001) (Zhao & Suo, 2010) (Mooney, 1940) (Ogden, 1972) (Gent, 1996) (Yeoh, 1990). However, it is difficult to have a general frame to combine all different models. There have been many studies and efforts to combine the hyperelastic material models and the theories of Maxwell stress

in the field of DEAs. Kofod (Kofod, 2001) used three different kinds of hyperelastic material models, (Ogden, neo-Hookean, and Hooke models) to describe a DEA relates to the one-dimensional voltage-strain.

Goulbourne et al (N. C. Goulbourne, Frecker, & Mockensturm, 2004) (N. Goulbourne, Mockensturm, & Frecker, 2005) developed a prosthetic blood pump using the Ogden strain energy function and an electro-elastic modeling of a DE-based diaphragm was employed. In (H. K. Kim et al., 2001), Kim et al studied the effects of parameters such as dielectric, pre-strain, temperature, and frequency, and with a MooneyRivlin model the relations of strain and stress was obtained by using elastic strain energy. Wissler and Mazza in (Wissler & Mazza, 2005) investigated a pre-strained dielectric elastomer with a circular membrane by employing three different hyperelastic strain energy models (Mooney-Rivlin, Yeoh, and Ogden).

In (Plante & Dubowsky, 2006), Plante and Dubowsky developed a model that accounts for DEAs failures like material strength, dielectric strength, and pull-in. In order to anticipate the DEAs' area stretch, the analytical model was incorporated four fundamentals parts including variable dielectrics strength, nonlinear elastic behavior, deformations, and viscoelasticity. The model was presented as a function of speed of actuation, working load, applied voltage, and mechanical prestretch. Suo and colleagues (Suo, 2010) (Hong, Zhao, & Suo, 2010) (Y. Liu, Liu, Zhang, & Leng, 2009) from Harvard University, America, presented a general theory to model the DEAs' electromechanical behaviors considering the framework of thermodynamics and continuum mechanics.

2.3.1.2 A General Electromechanical Modeling Frame

Figure 3.1 illustrates a DE membrane in its standard state with starting measurements of length L_1, width L_2, and thickness L_3. In the actuated state under mechanical forces P_1, P_2 and voltage Φ, the geometric dimensions become as l_1, l_2, and l_3, where the stretches on all directions are as $\lambda_1 = l_1/L_1$, $\lambda_2 = l_2/L_2$, and $\lambda_3 = l_3/L_3$. The membrane is assumed to be incompressible, and with density of ρ. For electrical attachment, the compliant electrodes are covered of grease on both surfaces of the membrane. Q refers to the electric charges on the electrodes, and the thermodynamic functioning of the transducer is assumed to be overly entropic, characterized by the Helmholtz free energy, which is denoted as F.

Frame Work of Equilibrium Thermodynamics:

The membrane of DE deforms due to the charges from the opposing signs on both electrodes, and the dimensions of the dielectric change by δl_1, δl_2, δl_3. As a result, the forces do work of $P_1\delta l_1$, $P_2\delta l_2$, and $P_3\delta l_3$. The work resulting from the mechanical forces $P_1\delta l_1 + P_2\delta l_2 + P_3\delta l_3$ and the work resulting from the battery $\phi\delta_Q$ is equivalent to the increase of the free energy of the elastomer membrane δF according to the energy balance, yields to:

$$\delta F = P_1\delta l_1 + P_2\delta l_2 + P_3\delta l_3 + \Phi\delta Q \tag{5}$$

It is worth to mention that the equilibrium state mentioned in (5) is used for random small changes of the four independent variables Q, l_1, l_2, and l_3 (Suo, 2010). The nominal density of the Helmholtz free energy is defined as:

$$W = F/(L_1L_2L_3) \tag{6}$$

Define the true stresses by:

$$\sigma_1 = P_1/(l_2l_3) \tag{7}$$

$$\sigma_2 = P_2/(l_1l_3) \tag{8}$$

$$\sigma_3 = P_3/(l_1l_2) \tag{9}$$

The electric field by:

$$E = V/l_3 \tag{10}$$

The electric displacement by:

$$D = Q/(l_1l_2) \tag{11}$$

The three quantities D, l_1, and l_2 are varied when the forces and voltage are applied, giving; ($\delta Q = Dl_2\delta l_1 + Dl_1\delta l_2 + l_1l_2\delta D$)

Consequently, by dividing (5) by the volume $L_1L_2L_3$ of the elastomer on the two sides, the overall

amount of increase in the density of the free energy can be accomplished.

$$\delta W = (\sigma_1 + DE)\lambda_2\lambda_3\delta\lambda_1 + (\sigma_2 + DE)\lambda_1\lambda_3\delta\lambda_2 + \sigma_3\lambda_1\lambda_2\sigma\lambda_3 + \lambda_1\lambda 2\lambda_3 E\delta_D \tag{12}$$

The nominal density of the Helmholtz free energy W is based on four independent variables, which are the strains l_1, l_2, l_3 and polarization displacement D, and it can be expressed as follows:

$$W = W(\lambda_1, \lambda_2, \lambda_3, D) \tag{13}$$

Submitting (13) into (12), we obtain:

$$\begin{aligned} W = &(\frac{\partial_W}{\partial_{\lambda_1}} - (\sigma_1 + DE)\lambda_2\lambda_3)\partial_{\lambda_1} \\ &+ (\frac{\partial_W}{\partial_{\lambda_2}} - (\sigma_2 + DE)\lambda_1\lambda_3)\partial_{\lambda_2} \\ &+ (\frac{\partial_W}{\partial_{\lambda_3}} - \sigma_3\lambda_1\lambda_2)\partial_{\lambda_3} \\ &+ (\frac{\partial_W}{\partial_D} - \lambda_1\lambda_2\lambda_3 * E)\partial_D \\ &= 0 \end{aligned} \tag{14}$$

The coefficients in front of each variations in eq. (14) can be derived when the dielectric is equilibrated under applying voltage and forces due to the fact that the balanced state in (5) is for random little differences of the four independent variables δl_1, δl_2, δl_3, and δD; satisfying:

$$\sigma_1 = \frac{\partial W(\lambda_1, \lambda_2, \lambda_3, D)}{\lambda_2\lambda_3\partial\lambda_1} - DE \tag{15}$$

$$\sigma_2 = \frac{\partial W(\lambda_1, \lambda_2, \lambda_3, D)}{\lambda_1\lambda_3\partial\lambda_2} - DE \tag{16}$$

$$\sigma_3 = \frac{\partial W(\lambda_1, \lambda_2, \lambda_3, D)}{\lambda_1\lambda_2\partial\lambda_3} \tag{17}$$

$$E = \frac{\partial W(\lambda_1, \lambda_2, \lambda_3, D)}{\lambda_1\lambda_2\lambda_3\partial D} \tag{18}$$

Ideal Dielectric Elastomers:

The change in volume is very small as comparison to the change in the shape when the dielectric elastomer is subjected to large deformation. As a result, the dielectric elastomers is assumed to be incompressible, which implies that the membrane volume is constant independently of the state of deformation (Suo, 2010), yields:

$$\lambda_1 \lambda_2 \lambda_3 = 1 \tag{19}$$

The density of the free energy of an incompressible elastic dielectric is based on the three independent variables:

$$W(\lambda_1, \lambda_2, D) \tag{20}$$

The actual electric displacement relates to the actual electric field is:

$$D = \varepsilon \times E \tag{21}$$

By assuming that the DEA has the ideal dielectric elastomer membrane, the nominal density of the Helmholtz free energy can be expressed as:

$$W(\lambda_1, \lambda_2, D) = W_s(\lambda_1, \lambda_2) + D^2/2\varepsilon \tag{22}$$

where $W_s(\lambda_1, \lambda_2)$ is the Helmholtz free energy related to the stretch amount of the membrane; $D_2/2\varepsilon$ represents the Helmholtz free energy related to the polarization of the elastomer, and the permittivity of the elastomer $\varepsilon = \varepsilon_0\ \varepsilon_r$ is a constant independent of deformation. Submitting eq. (22) into (15)-(18), the constitutive equations of DEAs will be as follows:

$$\sigma_1 - \sigma_3 = \frac{\lambda_1 \partial W_s(\lambda_1, \lambda_2)}{\partial \lambda_1} - \varepsilon E^2 \tag{23}$$

$$\sigma_2 - \sigma_3 = \frac{\lambda_2 \partial W_s(\lambda_1, \lambda_2)}{\partial \lambda_2} - \varepsilon E^2 \tag{24}$$

where the first terms of equations (23) and (24) indicate the mechanical stress part regarding the alteration of entropy related to the stretch of the elastomers' polymer network. The second term

implies the applied voltage. It should be mentioned that the model of ideal dielectric elastomers can be adjusted to include dissipative processes, such as electrical conduction, dielectric relaxation, and viscoelasticity (Zhao & Wang, 2014) (Zhou, Jiang, & Khayat, 2015).

2.3.1.3 Elastic Material Models

A hyperelastic constitutive material has a remarkable stress-strain relationship, which allows for accurately modeling it even when the strain is very large. The usefulness of Hyperelastic materials for modeling rubber-like or rubber materials has been approved in which the elastic deformation can be very large. By using a strain energy density function, hyberelastic materials can derive the stress-strain relationship. Different hyperelastic models have been developed and well-tested in theory of rubber-like materials modeling, such as neo-Hookean, Mooney-Rivlin, Yeoh, Gent, and Ogden models (Zhao & Suo, 2010) (Mooney, 1940) (Ogden, 1972) (Gent, 1996) (Yeoh, 1990). A specific model can be chosen based on some categories. For example, the amount of data that has to define the relationship between the stress and strain, the computational expense of the formulation, and the expected range of strains that will be experienced. In the field of DEAs, Ogden, neo-Hookean, and Gent models are the commonly used due to their simplicity, which they are introduced In this paper.

Ogden Model:

For rubber elasticity, Ogden model is also one of the popular hyperelastic material models, and it was proposed by Raymond Ogden in 1972 (Ogden, 1972). Ogden model is usable for describing the non-linear stress-strain behavior of specific materials such as polymer or rubber-like materials. The strain energy density function of Ogden model can be derived, like other hyperelastic material models, to describe the behavior of the material. In Ogden material model, the strain energy density under the assumption of incompressibility one can be written as:

$$W_s = \sum_{i=1}^{N} \frac{\mu i}{\alpha_i} (\lambda_1^{\alpha_i} + \lambda_2^{\alpha_i} + \lambda_3^{\alpha_i} - 3) \tag{25}$$

where N is the number of model order, and μ_i and α_i are the parameters of the material, which can be verified by experiments. Unlike the other models (Neo-Hookean model, Gent model), Ogden

model has the advantages of directly using the test data without the exact physical meaning of the material. In contrast, the parameters of Gent model and Neo-Hookean model have physical description for the materials, which make them physical-based models. In addition, Ogden model can be effectively used to examine the performance of DEAs due to the high ability to predict the response of DEAs (Y. Liu et al., 2009) (Joglekar, 2014) (Ahmadi, Gooyers, Soleimani, & Menon, 2013) (Zhou et al., 2015).

Neo-Hookean Model:

Neo-Hookean is considered as hyperelastic model; and for the case of large deformations, Neo-Hookean is an extension of Hookes law. In 1948, Ronald Rivlin proposed the neo-Hookean model, and it is used for rubber-like substances and certain plastics (Mooney, 1940) (Suo, 2010) (Kofod, 2001) (Zhao & Suo, 2010) (Mooney, 1940) (Ogden, 1972) (Gent, 1996) (Yeoh, 1990). For an incompressible neo-Hookean hyperelastic material, the free energy density is given by:

$$W_s = \frac{\mu}{2}(\lambda_1^2 + \lambda_2^2 + \lambda_3^2 - 3) \tag{26}$$

where μ is a material constant (associated with Youngs modulus), which is the strain shear modulus. The neo-Hookean model has the advantage of predicting the stress-strain behavior of hyperelastic materials undergoing large deformation. In dielectric elastomers (DEs), the curve of stress-strain in a neo-Hookean material is initially linear; however, at a certain point the relation between the applied stress and strain may change to nonlinear.

The bases of a neo-Hookean model are the statistical thermodynamics of cross-linked polymer chains, and it is one of the simple models with only one material parameter μ. In a Neo-Hookean manner, Cross-linked polymers perform in the linear states. However, the length of each polymer chain could be limited, and the polymer chains will be stretched to the maximum point at a certain point, which the covalent crosslinks will allow. Consequently, the elastic modulus of the material will dramatically increase, and may also cause the elastomer to stiffen sharply. Thus, at large strains, the neo-Hooken model is not accurately practical.

Gent Model:

Gent model is a hyperplastic model of rubber elasticity, and it was introduced by Gent in 1996 (Gent, 1996). The benefit of this model is predicting the strain-stiffening effect unlike the neo-Hookean model. Gent model for isotropic incompressible elastomers is particularly simple, and it can be expressed as follows:

$$W_s = -\frac{\mu J_{lim}}{2} ln\left(1 - \frac{\lambda_1^2 + \lambda_2^2 + \lambda_3^2 - 3}{J_{lim}}\right) \tag{27}$$

In a similar way to the neo-Hookean model in (26), μ refers to the small-strain shear modulus, and J_{lim} refers to the limiting stretch, and generally has a constant value and can express the effects resulting from strain-stiffening of materials.

According to the Taylor expansion, Gent model can be reduced to Neo-Hookean solid model, and this can be seen when $\lambda_1^2 + \lambda_2^2 + \lambda_3^2 - 3/J_{lim} \to 1$. As a result, the elastomer meets its maximum limiting stretch point, and the free energy W_s will be diverged. For predicting the behaviors of DEAs, Gent model has become one of the most widely used models at the current time (Kollosche, Zhu, Suo, & Kofod, 2012) (Zhu, Kollosche, Lu, Kofod, & Suo, 2012) (N. Goulbourne et al., 2005). Since Gent model is remarkably uncomplicated with only two material parameter μ and J_{lim}, and since it can predict the stiffing-strain, it is thus an excellent alternative to the comparatively complicated models for incompressible rubber-like materials modeling.

2.3.2 Considering the Viscoelasticity

Dissipative processes, suchlike current leakage, dielectric relaxation, and viscoelasticity influence the dynamic performance and electromechanical energy conversion of dielectric elastomer actuators. The dielectric elastomer is usually subjected to voltages, transients and time-dependent forces in order to act as an actuator. Therefore, the mechanisms of dissipation in the system will affect the performance of DEAs. For instance, the actuation of DEAs can be adversely affected by viscoelasticity and current leakage according to experimental studies, which would limit its applicable applications (Hong, 2011) (Plante & Dubowsky, 2007) (Molberg et al., 2009) (Zhou et al., 2015). Thus, in order to accurately model a DEA, viscoelasticity has to be accounted for. Four types

of variables can describe the state of equilibrium dielectric elastomer actuators, which are charge, force, voltage and displacement.

In a characteristic time, the dielectric elastomer is relaxed and changes to a new type of deformation when it is subjected to a mechanical force, named as the viscoelastic relaxation time τ_V. In a dielectric elastomer, the relaxation to a new state of polarization highly depends on temperature, and it mainly happens when a dielectric elastomer undergoing voltages over a characteristic time; this case commonly called as the dielectric relaxation time τ_d. Subject to a power source, some current could flow over the dielectric, which is called current leakage. In a nonequilibrium thermodynamics framework, the work resulting from the battery ($\Phi\delta_Q$) and the total work resulting from the mechanical forces ($P_1\delta l_1 + P_2\delta l_2 + P_3\delta l_3$) should be greater or equal to the increase of the free energy F; denoted as:

$$\delta_F \leq P_1\delta l_1 + P_2\delta l_2 + P_3\delta l_3 + \Phi\delta_Q \tag{28}$$

Considering the density of the free energy W as mentioned in (6), the thermodynamic inequality becomes:

$$\delta W \leq (\sigma_1 + ED)\lambda_2\lambda_3\delta\lambda_1 + (\sigma_2 + ED)\delta\lambda_1\lambda_3\delta\lambda_2 + \sigma_3\lambda_1\lambda_2\delta\lambda_3 + \lambda_1\lambda_2\lambda_3 E\delta D \tag{29}$$

The dielectric elastomer is taken to be incompressible, so that $l_1l_2l_3 = L_1L_2L_3$ and $\lambda_1\lambda_2\lambda_3 = 1$. the free-energy density is prescribed as a function:

$$W(\lambda_1, \lambda_2), D, \xi_A, \xi_B \tag{30}$$

The state of a dielectric elastomer can be characterized by λ_1 and λ_2, D, and ξ_A,ξ_B. These additional parameters ξ_A, ξ_B represent the degrees of freedom related to dissipative processes effects in the dielectric elastomers, and are known as internal variables. For the model of ideal dielectric elastomers, the density of the Helmholtz free energy W can be rewritten as:

$$W(\lambda_1, \lambda_2, D, \xi_A, \xi_B), ... = W_{stretch}(\lambda_1, \lambda_2, \xi_A, \xi_B, ...) + \frac{D^2}{2\varepsilon} \tag{31}$$

where $W_{stretch}$ is the Helmholtz free energy associated with the stretching of the elastomer. Combining Eq. (29) and (31) resulting:

$$\left(\frac{\partial W}{\partial \lambda_1} - (\sigma_1 + DE)\lambda_2\lambda_3\right)\delta\lambda_1 + \left(\frac{\partial W}{\partial \lambda_2} - (\sigma_2 + DE)\lambda_1\lambda_3\right)\delta\lambda_2 + \left(\frac{\partial W}{\partial \lambda_3} - \sigma_3\lambda_1\lambda_2\right)\delta\lambda_3 + \left(\frac{\partial W}{\partial D} - E\right)\delta D + \sum_{\gamma}\frac{\partial W_{stretch}}{\partial \xi_\gamma}\delta\xi_\gamma \leq 0 \tag{32}$$

Assuming that the system is in electrostatic and mechanical equilibrium, so that in (32) the variables in front of δl_1, δl_2,δl_3 and δD disappear:

$$\sigma_1 - \sigma_3 = \lambda_1\frac{\partial W_{stretch}(\lambda_1, \lambda_2, \xi_A, \xi_B, ...)}{\partial \lambda_1} - \varepsilon E^2 \tag{33}$$

$$\sigma_2 - \sigma_3 = \lambda_2\frac{\partial W_{stretch}(\lambda_1, \lambda_2, \xi_A, \xi_B, ...)}{\partial \lambda_2} - \varepsilon E^2 \tag{34}$$

Once the elastomer is assumed to be in electrostatic and mechanical equilibrium, the inequality in Eq. (32) becomes:

$$\sum_{\gamma}\frac{\partial W_{stretch}(\lambda_1, \lambda_2, \xi_A, \xi_B, ...)}{\partial \xi_\gamma}\delta\xi_\gamma \leq 0 \tag{35}$$

Recently, viscoelastic dielectrics have been theoretically investigated by a rheological model consisting of springs and dashpots with several parallel units as illustrated in figure 3.3. Where the first unit includes an elastic spring, and the rest of units include elastic springs together with several viscoelastic units; the elastic springs are in series with viscous dashpots. In order to describe the elastic springs, the elastic material models can be simply built by connecting the simplest rheological elements, springs and dashpot elements, in series or parallel (Kollosche, Kofod, Suo, & Zhu, 2015) (Zhou et al., 2015) (Park & Nguyen, 2013) (Sheng, Chen, Li, & Wang, 2014) (Chiang Foo et al., 2012).

2.3.3 Considering the Dynamic Behavior

The development of dielectric elastomer actuators and their industrial applications are intense, and they grow intensely as electromechanical transducers (R. Pelrine et al., 2000). In the past, the use of DEAs in areas such as programmable haptic surfaces, energy harvesting, adaptive optics, and soft robots got attention of many researchers, and a large number of studies have been strongly interested in the quasi- static behavior of large-deformation that DEAs are known for. Nevertheless, the effects of inertia and damping has been ignored (Kofod, 2001). However, DEAs have the advantage of deforming over different frequencies. The dynamic behavior of DEAs is of great significance when it comes to modeling, and has attracted significant attention in the robotics society. In recent years, the dynamic responses of DEAs have become an attractive subject, and not many studies have been done to study it.

In 2008, Dubois et al. demonstrated that a voltage can tune the frequency of a flat membrane of dielectric electroactive polymer (DEAP). Zhu et al. (2010) (Zhu, Cai, & Suo, 2010) study nonlinear oscillation of a pre- stretched dielectric elastomer with a spherical membrane, and the results show that the membrane experiences harmonic resonance, superharmonic resonance as well as subharmonic. In a similar way, Li et al (Li, Qu, & Yang, 2012) study a prestretched dielectric elastomer when subjected to combined loads of voltage cycles and tensile forces. An in-plane one-dimensional DEA with an analytical dynamic model was then developed and represented. They found that the natural frequency of DEAs can be tuned by applied static voltages and pre- stretches, and the dynamic behavior of the DEA can also be modified. Feng et al (Feng, Yu, & Zhang, 2014) use the squeeze-film theory to investigate the dynamic performance of a DE microbeam resonator.

According to the Euler-Bernoulli beam model, estimated analytical solutions can be obtained to analyze the resonator efficiency, such as the frequency shift ratio and the Q-factor. Moreover, it is also concluded that constructing resonators using DEs can achieve the active frequency tuning. For a particular amount of ambient pressure, the proposed analytical model is proved to be reasonable and applicable. Based on the Euler-Lagrange equations, there is another method to evaluate the dynamic evaluation of a homogeneously deformed DEA, which is presented by Xu et al (Xu, Mueller, Theis, Klassen, & Gross, 2012). In (Zhang et al., 2015) Chi Zhang et al. initiate the kinetic equation of an

active hinge configuration actuated by a dielectric elastomer for theoretically investigating the static and dynamic performance. They found that when subjecting the hinge to a constant voltage, it can rotate to an equilibrium state.

The state of equilibrium is affected by prestretch ratios and the modes of deformation of the DE. The importance of investigating the functioning of the hinge configuration is that it can be a guide to design the configuration in dynamic field, which effectively increases the structure's application fields. The reported work in (Zhu et al., 2010) investigated theoretically the nonlinear dynamics of a membrane of a dielectric elastomer with taking into account the resonant response, where the membrane is constructed over a rigid ring, filled with a voltage and a pressure into an axisymmetric form. The dynamic performance of the DEA with the nonlinear electromechanical equation was studied by Kaal and Herold, and the simulation model developed is validated to effectively represent the actuator performance and to investigate the control loop, the mechanical structure, and its interaction with the amplifier (Kaal & Herold, 2011).

Similarly, in (Rosset & Shea, 2013) Rosset et al investigated the dynamic response of the DEAs, which was further verified in experiments. Their experimental results showed that there is a strong relationship between the dynamic response of the DEAs and membrane material together with compliant electrodes. To describe the relationship between the stress and strain in DEAs, Sarban et al established an ordinary differential equation of a fourth-order (Sarban, Lassen, & Willatzen, 2012). The speed of response in DEAs as well as the response of DEAs during cyclic loading and unloading voltages are important aspects, especially for applications that demand actuators have the ability to change deformations rapidly and repeatedly.

The reported works in (Sarban et al., 2012) (Gu et al., 2017) (Kaal & Herold, 2011) have attempted to investigate the dynamic response and nonlinear electromechanical phenomena in DEAs to a better understanding of its dynamic behavior. It can be concluded that understanding dynamic electromechanical model of a DE actuator is extremely significant for technological development in soft robotics. In the robotics society, the analysis of the dynamic behaviors of the DEAs has become the focus of interest. Nonetheless, understanding the physical aspect of the dynamic behaviors of DEAs is still an open case, and has not been completely proposed.

2.4 Influence of Temperature on DE

Temperature influences the performance of dielectric elastomers, and the thermal impact on the DEs behavior is widely reported to be crucially essential. More importantly, the electromechanical deformation of viscoelastic dielectric elastomers (DEs) is strongly affected by three material parameters, which are relaxation time, Young's modulus, and permittivity, and all the three parameters are associated with temperature. The high nonlinearity in the actuation is observed for material, such as the one used in this study the dielectric acrylic elastomer VHB 4910. Silvain-Michel et al (Michel et al., 2010) investigated the material properties of the 3M acrylic elastomer. They found that the VHB-based DEs display strong temperature dependency.

According to Sahu and Patra (Sahu et al., 2015) (Patra & Sahu, 2015), there is a strong relationship between this material's strain, creep, stress relaxation and loading conditions such as the holding strain, the holding stress, and the loading rate, even at room temperature. In Jean-Mistral et al. study (Jean-Mistral, Sylvestre, Basrour, & Chaillout, 2010), the stress due to electrostriction highly depends on the temperature and deformation dependent dielectric constant, and contribute to develop the state of equilibrium of the dielectric elastomer. Therefore, the understanding of the temperature influence on a DE material becomes more intriguing, and a complete description of such a nonlinear material DEs behavior must take the thermal impact into account.

Many researchers have conducted an investigation into the influence of external factors such as frequency, type of electrodes, pre-stretch, electrical field on the dielectric constant of VHB 4910 (Sommer-Larsen, Kofod, Shridhar, Benslimane, & Gravesen, 2002) (H. K. Kim et al., 2001). In the current literature, based on the findings, the ambient temperature highly impacts the mechanical behavior of VHB-based DEs and their dielectric properties, especially their strain-stress relationship. Jean-Mistral et al. indicated that the dielectric constant decreases as the temperature increases at a low frequency of $0.1Hz$. They also found that when the temperature escalates from $-50°$C to $75°$C, the elastic modulus of a DE changes by over two orders of magnitude (Jean-Mistral et al., 2010) (Vu-Cong, Jean-Mistral, & Sylvestre, 2013).

Moreover, the shear modulus and the dielectric constant of DEs have shown a deformation and temperature-dependence behavior (Jean-Mistral et al., 2010) (Sheng, Chen, Li, & Chang, 2013).

Meanwhile, the temperature has also an influence on the dynamic performance of a DE and its viscoelastic relaxation (Sheng et al., 2013). Furthermore, the impact of temperature on the electromechanical actuation is also observed for pre-stretched DEs with viscoelastic behaviour (L. Liu et al., 2015). Having an understanding of these thermal effects on the DEs actuators, especially for applications in environments in which temperature varies, is significantly important.

2.5 Influence of Pre-stretch on DE

Dielectric elastomers have shown their capability of large voltage-induced deformation and giant electromechanical actuation. However, it is a major challenging to successfully achieve such large deformation in practice due to electromechanical instability, such as pull-in, snap through, and electric breakdown. A stabilized large actuation can be obtained by applying a mechanical pre-stretch. The mechanical pre-stretch is practical to stabilize the dielectric elastomer in several ways, by enhancing the breakdown strength, by producing electrostriction, by removing the pull-in instability, and by decreasing the thickness of the membrane which consequently reduces the voltages required for activation.

Dielectric elastomers (DEs) exhibits electromechanical instability (EMI), which is one of its commonly known failures. Electromechanical instability (EMI) limits the effective investigation of the very large deformation that dielectric elastomers are known for, and blocks the maximum strain in the direction of the thickness (Zhao & Suo, 2008) (Zhao & Suo, 2009). The mechanical stress occurs because of the squeezing force that comes from the attraction of the dielectric elastomers' electrodes. When the mechanical stress is more than the compressive stress of the elastomer membrane, which is unstable due to the dielectric's elasticity, then the electromechanical instability (EMI) or pull-in instability happens (Zhao & Wang, 2014).

Snap-through instability can also affect the actuation of DEs. It occurs when the dielectric elastomer get through the electromechanical instability without electrical breakdown, and at a constant voltage simultaneously experience a coexistence of two states: thick and thinner stable membrane with a much smaller thickness (Zhao, Hong, & Suo, 2007). As a boundary condition, the mechanical pre-stretch of the dielectric elastomer was theoretically investigated by Zhao and Suo (Suo, 2010).

They presented a free energy model by using Neo-Hookean strain energy function, which can predict the pull-in instability. The deformation and the dielectric constant for an acrylic elastomer VHB tape, commercially available from 3M company, are closely related (Kofod, 2001). Meaning that in the actuation of the DEs, electrostriction will be generated, and consequently affect the stabilization of the DEs (Jiang, Betts, Kennedy, & Jerrams, 2016).

In (Zhao & Wang, 2014), Zhao investigated the pull-in instability using a polyacrylate DE tape (VHB 4910, 3M) and the results show that if the soft DEs stiffen adequately under deformations, pull-in instability can be effectively removed. Therefore, pre-stretch is a significantly practical way to eliminate the electromechanical instability from DEs mostly due to the strain stiffening impact. For stabilization on dielectric elastomrs, the mechanical pre-stretch not only eliminates the pull-in instability but also sufficiently affects the voltage-induced strain of all DEs' films. The experimental results done by Pelrine et al. (R. Pelrine et al., 2000) show that by employing an equi-biaxial pre-stretch ratio of 3 on the VHB 4910 film, it can reach a large voltage-induced strain of up to 158%.

At a pre-stretch ratio of 2 for VHB 4910 films, it was reported that a maximum voltage-induced strain of 200% can be achieved by applying a large electric field (Jiang et al., 2016). Tuning the stiffness of a DE material can be achieved by applying pre-stretch; therefore, the mechanical pre-stretch affect the properties of a dielectric elastomer mechanically and dielectrically, resulting in a total stabilization improvement. Hence, it is necessarily important to establish a suitable model to characterizing the mechanical performance of DEs, and to study how the mechanical pre-stretch influences the stabilization of dielectric elastomer actuation.

Chapter 3

The Dynamic Model of a Dielectric Elastomer

3.1 The Elastic Energy

The thermodynamic system consists of the dielectric elastomer, the elastic energy, thermal energy, and the electric energy. In this sense, the free energy W can be prescribed as a function of the four independent variables λ_1,λ_2,T,D (Zhao & Suo, 2007), which describe the state of the elastomer. The membrane of dielectric elastomer (DE) is sandwiched between two compliant electrodes as illustrated in Figure3.1. Applying a voltage causes the dielectric elastomer to shrink in thickness and expand in area due to Maxwell stress (L. Liu et al., 2011) (Sheng, Chen, & Li, 2011). In the undeformed state, dimensions of the membrane are L_1, L_2 and L_3, while the corresponding dimensions of the membrane after deformation are l_1, l_2 and l_3, (See Figure 3.1, 3.2). In a deformed state, the DE would be subjected to forces P_1 and P_2, and an electric voltage ϕ is applied through the thickness and between the two electrodes with an environment of a fixed temperature T. We define the stresses by the mechanical forces divided by the area of the elastomer in the undeformed state $\sigma_1 = \frac{P_1}{L_2 L_3}$ and $\sigma_2 = \frac{P_2}{L_1 L_3}$, the nominal electric field by the voltage in the deformed state divided by the thickness of the elastomer in the undeformed state $E = \frac{\phi}{L_3}$. Also, the stretches can be addressed as $\lambda_1 = \frac{l_1}{L_1}$ and $\lambda_2 = \frac{l_2}{L_2}$, and the nominal electric displacement as the charge on an electrode in the deformed state divided by the area of the electrode in the undeformed state $D = \frac{Q}{L_1 L_2}$.

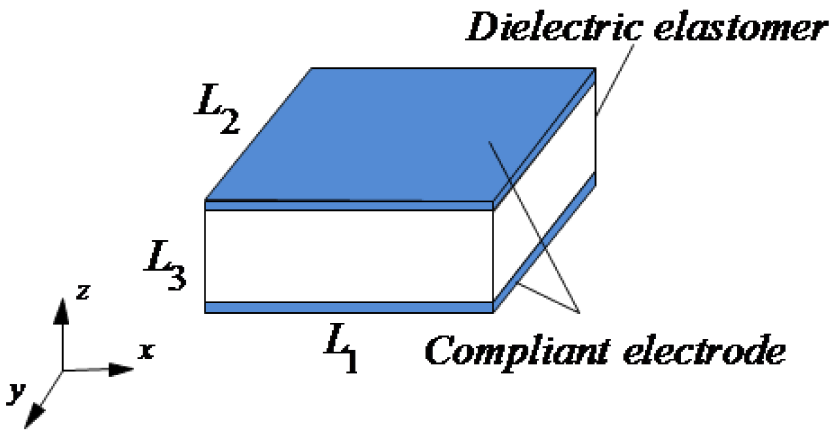

Figure 3.1: (a) Undeformed state of DE.

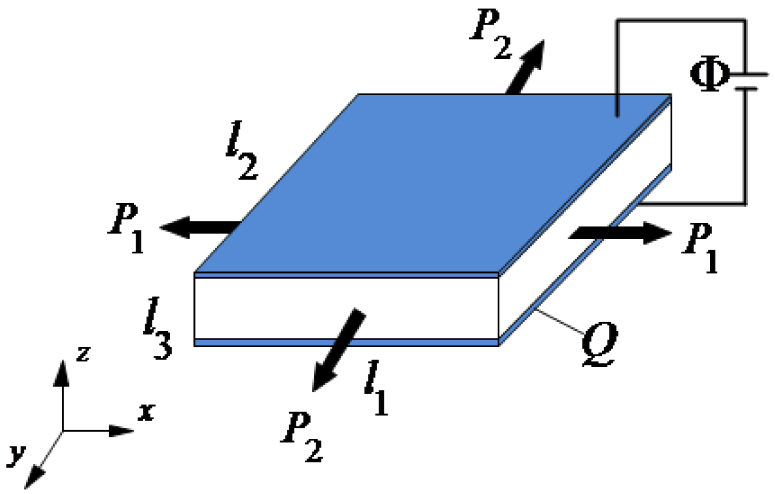

Figure 3.2: (b) Deformed state of DE.

In practice, the Gent model has the advantage of predicting the strain-stiffening effect and approaching the dielectric elastomer limiting stretch, which was introduced by Gent in 1996 (Gent, 1996). To account for the extension limits, the Gent model is chosen to describe the isothermal free energy density $W_s(\lambda_1\lambda_2)$ (Bilgili, Bernstein, & Arastoopour, 2001) (Plante & Dubowsky, 2006) (Gent, 1996).

$$W_s = -\frac{\mu J_{\lim}}{2} \ln\left(1 - \frac{\lambda_1^{-2} + \lambda_2^{-2} + \lambda_1^{-2}\lambda_2^{-2} - 3}{J_{\lim}}\right) \tag{36}$$

where μ is the small-strain shear modulus, and $J_{\lim}$ is the limiting stretch constant, which can describe the strain-stiffening effect.

3.2 The Thermal Energy

The thermal part can be described as $H(T) = Q(T) - TS$ where $Q(T)$ is the internal energy. When the temperature increases, the internal energy is expressed as $Q(T) = \rho_0 c_0[T - T_0]$. The laws of thermodynamics imply the following relation between specific heat for constant volume and entropy (Gu et al., 2017), $\rho_0 = T\frac{\partial S}{\partial T}$. It follows, $S = \rho_0 \ln \frac{T}{T_0}]$ where the parameters ρ_0 and c_0 denote the mass density and the specific heat Capacity (Bilgili et al., 2001), T_0 is the reference temperature, and T refers to an environment of a fixed temperature. Therefore, the expression that reflects the effect of temperature on the free energy of the thermodynamic system can be obtained as follows:

$$H(T) = \rho_0 c_0 \left[-T_0 - T \ln \frac{T}{T_0}\right] \tag{37}$$

3.3 The Electric Energy

The expression of electric displacement relates to the electric field is given by $D = \varepsilon E$, where the permittivity of the elastomer is $\varepsilon = \varepsilon_0 \varepsilon_r$. For an ideal dielectric elastomer, the dielectric energy per unit volume is $\frac{D^2}{2\varepsilon}$.

According to Suo (Suo, 2010), by considering the electrostriction of dielectric elastomers, the electrostatic energy takes the form of $\frac{D^2}{2\varepsilon_0 \epsilon_r}\lambda_1^{-2}\lambda_2^{-2}$. Since we use voltage in our experiment, the electric displacement can be replaced by voltage, and the dielectric energy can be rewritten as follows:

$$W_{ele} = \frac{\varepsilon(\lambda_1, \lambda_2, T)}{2}\left(\frac{\Phi}{L_3}\right)^2 \lambda_1^2 \lambda_2^2 \tag{38}$$

3.4 The Dynamic Model of a DE

By combining the three elements, the elastic energy, thermal energy, and the electric energy, we obtain the free energy model of the thermodynamic system as:

$$W = W_{ela} + W_{he} + W_{ele} \tag{39}$$

$$W = -W_s(\lambda_1\lambda_2) + \rho_0 c_0 \left[-T_0 - T\ln\frac{T}{T_0}\right] + \frac{\varepsilon(\lambda_1,\lambda_2,T)}{2}\left(\frac{\Phi}{L_3}\right)^2 \lambda_1^2\lambda_2^2 \tag{40}$$

where the first term of equation (40) is the elastic energy (Suo, 2010) (Bilgili et al., 2001), and the second term is the purely thermal contribution, where $H(T)$ indicates the thermal contribution, in which the thermodynamic system is denoted by the influence of the temperature of the free energy. The third term is the dielectric energy; where $\varepsilon_0 = 8.85 * 10^{-12} Fm^{-1}$ is the dielectric constant of Vacuum permittivity, ε_r is the temperature and deformation dependence of dielectric constant of the polymer, and represents the electric displacement.

By combining Eq. (36), Eq. (37), and Eq. (38), Eq. (40) can be rewritten as:

$$\begin{aligned} W = &-\frac{\mu J_{\lim}}{2}\ln\left(1 - \frac{\lambda_1^2 + \lambda_2^2 + \lambda_1^{-2}\lambda_2^{-2} - 3}{J_{\lim}}\right) \\ &+ \rho_0 c_0 \left[-T_0 - T\ln\frac{T}{T_0}\right] + \frac{\varepsilon(\lambda_1,\lambda_2,T)}{2}\left(\frac{\Phi}{L_3}\right)^2 \lambda_1^2\lambda_2^2 \end{aligned} \tag{41}$$

Remark1.

Relative permittivity of the VHB elastomer is influenced by the temperature and stretch simultaneously. According to the research of Jean-Mistral (Jean-Mistral et al., 2010), the expression of the temperature and deformation dependence of the permittivity of the DE is $\varepsilon = \varepsilon(T,\lambda) = a\lambda^2 + \frac{b}{T} + c$. Based on the experimental results of Jean-Mistral, the fitting parameters $a = 0.0533 Fm^{-1}$, $b = 645.4224 FKm^{-1}$, and $c = 3.1834 Fm^{-1}$ (Jean-Mistral et al., 2010).

The dielectric elastomer is taken to be incompressible, implying that the volume of the material remains unchanged during deformation; thus:

$$\lambda_1\lambda_2\lambda_3 = 1 \tag{42}$$

In order to describe the viscoelasticity of the DE, the general Kelvin-Voigt model is applied in this model. It includes five units, which are $(\alpha_0, \alpha_1, \alpha_2, \alpha_3, \alpha_4)$. The first unit (α_0) is a nonlinear spring describes the equilibrium state. The other units $(\alpha_i, i = 1, 2, 3, 4)$ are nonlinear springs with linear dashpots to detect the nonlinear time-dependent variation of the equilibrium state. Including several of parallel springs and dashpots adds more accuracy to the model, which can effectively predict the dynamic behavior of the DE such as the creep. Also, the constitutive model is based on the basis of nonequilibrium thermodynamics, and it is used to take into account the time-dependent response of the DEA.

Let $\xi(i = 1, 2)$ be the stretch due to the dashpot, the stretch of spring is determined by the multiplication rule as $\frac{\lambda_i^e}{\xi_i}$.

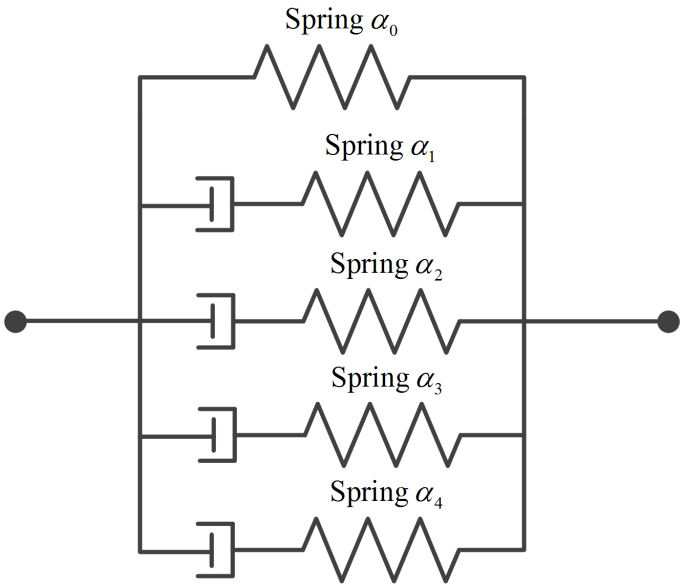

Figure 3.3: Schematic representation of five units Kelvin-Voigt model describing viscoelasticity.

Together with the rheological model, the elastic energies, thermal energy, and the electric energy, the detailed expression of the free energy function in this study can be expressed as follows:

$$W = W_{ela}^{\alpha_0} + W_{ela}^{\alpha_1} + W_{ela}^{\alpha_2} + W_{ela}^{\alpha_3} + W_{ela}^{\alpha_4} + W_{he} + W_{ele} \tag{43}$$

where $W_{ela}^{\alpha_0}$ is the elastic energy for the spring α_0, $W_{ela}^{\alpha_1}$ is the elastic energy for the spring α_1, $W_{ela}^{\alpha_2}$ is the elastic energy for the spring α_2, $W_{ela}^{\alpha_3}$ is the elastic energy for the spring α_3, $W_{ela}^{\alpha_4}$ is the elastic energy for the spring α_4, W_{he} is the purely thermal contribution, and W_{ele} is the electric energy.

$$\begin{aligned} W = & -\frac{\mu^{\alpha_0} J_{\lim}^{\alpha_0}}{2} \ln\left(1 - \frac{\lambda_1^2 + \lambda_2^2 + \lambda_1^{-2}\lambda_2^{-2} - 3}{J_{\lim}^{\alpha_0}}\right) \\ & - \sum_{i=1}^{4} \frac{\mu^{\alpha_i} J_{\lim}^{\alpha_i}}{2} \ln\left(1 - \frac{\lambda_1^2\xi_{i1}^{-2} + \lambda_2^2\xi_{i2}^{-2} + \lambda_1^{-2}\xi_{i1}^2\lambda_2^{-2}\xi_{i2}^2 - 3}{J_{\lim}^{\alpha_i}}\right) \\ & + \rho_0 c_0 \left[-T_0 - T\ln\frac{T}{T_0}\right] + \frac{\varepsilon(\lambda_1, \lambda_2, T)}{2}\left(\frac{\phi}{L_3}\right)^2 \lambda_1^2\lambda_2^2 \end{aligned} \tag{44}$$

where $W_{ela}^{\alpha_i}$ $(i = 1, 2, 3, 4)$ are elastic energy densities of the spring α_i; respectively, $W_{ela}^{\alpha_0}$ is the elastic energy for the spring α_0, μ^{α_0} and μ^{α_i} being the shear modulus of the spring α_0 and the spring α_i, respectively; $\rho_0 c_0$ is the specific heat capacity of the DE; $J_{\lim}^{\alpha_0}$ and $J_{\lim}^{\alpha_i}$ are deformation limits of the spring α_0 and the spring α_i, respectively.

Considering the fact that the condition of equilibrium thermodynamics dictates that the free energy system should be minimized (Jean-Mistral et al., 2010) (Sheng et al., 2013). As a result, the nominal stress, nominal electric field and specific entropy can be expressed via the partial derivative of free energy function W as:

$$\begin{aligned} \frac{\partial W}{\partial \lambda_1} = & -\frac{\mu^{\alpha_0}(\lambda_1 - \lambda_1^{-3}\lambda_2^{-2})}{1 - \frac{\lambda_1^2 + \lambda_2^2 + \lambda_1^{-2}\lambda_2^{-2} - 3}{J_{\lim}^{\alpha_0}}} - \sum_{i=1}^{4} \frac{\mu^{\alpha_i}(\lambda_1\xi_{i1}^{-2} - \lambda_1^{-3}\lambda_2^{-2}\xi_{i1}^2\xi_{i2}^2)}{1 - \frac{\lambda_1^2\xi_{i1}^{-2} + \lambda_2^2\xi_{i2}^{-2} + \lambda_1^{-2}\lambda_2^{-2}\xi_{i1}^2\xi_{i2}^2 - 3}{J_{\lim}^{\alpha_i}}} \\ & + \varepsilon(\lambda_1, \lambda_2, T)\left(\frac{\Phi}{L_3}\right)^2 \lambda_1\lambda_2^2 \end{aligned} \tag{45}$$

$$\begin{aligned} \frac{\partial W}{\partial \lambda_2} = & -\frac{\mu^{\alpha_0}(\lambda_2 - \lambda_1^{-2}\lambda_2^{-3})}{1 - \frac{\lambda_1^2 + \lambda_2^2 + \lambda_1^{-2}\lambda_2^{-2} - 3}{J_{\lim}^{\alpha_0}}} - \sum_{i=1}^{4} \frac{\mu^{\alpha_i}(\lambda_2\xi_{i2}^{-2} - \lambda_1^{-2}\lambda_2^{-3}\xi_{i1}^2\xi_{i2}^2)}{1 - \frac{\lambda_1^2\xi_{i1}^{-2} + \lambda_2^2\xi_{i2}^{-2} + \lambda_1^{-2}\lambda_2^{-2}\xi_{i1}^2\xi_{i2}^2 - 3}{J_{\lim}^{\alpha_i}}} \\ & + \varepsilon(\lambda_1, \lambda_2, T)\left(\frac{\Phi}{L_3}\right)^2 \lambda_1^2\lambda_2 \end{aligned} \tag{46}$$

The relationship between the charge Q and the voltage Φ is (Li et al., 2012),

$$Q = \Phi C = \Phi\frac{\varepsilon(\lambda_1, \lambda_2, T) l_1 l_2}{l_3} = \Phi\frac{\varepsilon(\lambda_1, \lambda_2, T)\lambda_1^2\lambda_2^2}{L_3/L_1L_2} \tag{47}$$

where $\varepsilon(\lambda_1, \lambda_2, T)$ is the permittivity of the DE, which is a nonlinear function of λ_1, λ_2 as well as the current environment temperature T, and C is the capacitance of the DE.

The dimensions of the DE change by $\delta\lambda_1, \delta\lambda_2, \delta\lambda_3$ (Gaskell & Laughlin, 2017); as a result, the tensile forces do work of $P_1 L_1 \delta\lambda_1$ and $P_2 L_2 \delta\lambda_2$. In addition, the change of the charge on the electrode δQ leads the voltage applied to do the work of $\Phi\delta Q$. Thus, the variation of the charge Q is:

$$\begin{aligned}\delta Q = &\frac{\epsilon(\lambda_1, \lambda_2, T)\lambda_1^2\lambda_2^2}{L_3/L_1L_2}\delta\Phi + 2\Phi\frac{\varepsilon(\lambda_1, \lambda_2, T)\lambda_1\lambda_2^2}{Ł_3/L_1L_2}\delta\lambda_1 \\ &+ 2\Phi\frac{\varepsilon(\lambda_1, \lambda_2, T)\lambda_1^2\lambda_2}{L_3/L_1L_2}\delta\lambda_2 + \Phi\frac{\lambda_1^2\lambda_2^2}{L_3/L_1L_2}\frac{\partial\varepsilon(\lambda_1, \lambda_2, T)}{\partial\lambda_1}\delta\lambda_1 \\ &+ \Phi\frac{\lambda_1^2\lambda_2^2}{L_3/L_1L_2}\frac{\partial\varepsilon(\lambda_1, \lambda_2, T)}{\partial\lambda_2}\delta\lambda_2 + \Phi\frac{\lambda_1^2\lambda_2^2}{L_3/L_1L_2}\frac{\partial\varepsilon(\lambda_1, \lambda_2, T)}{\partial T}\delta T\end{aligned} \tag{48}$$

The inertia forces in each material element along the x-direction, y-direction and z-direction respectively are $\rho L_2 L_3 x^2(d^2\lambda_1/dt^2)$, $\rho L_1 L_3 y^2(d^2\lambda_2/dt^2)$, $\rho L_1 L_2 z^2(d^2\lambda_3/dt^2)$, where ρ is the density of the DE. Consequently, the total work done by the inertia forces can be integrated along each direction as follows (Gaskell & Laughlin, 2017):

$$\rho L_2 L_3 x^2 \frac{d^2\lambda_1}{dt^2}\delta\lambda_1 \int_0^{L_1} x^2 dx = \frac{L_1^3 \rho L_2 L_3}{3}\frac{d^2\lambda_1}{dt^2}\delta\lambda_1 \tag{49}$$

$$\rho L_1 L_3 y^2 \frac{d^2\lambda_1}{dt^2}\delta\lambda_1 \int_0^{L_2} y^2 dx = \frac{L_2^3 \rho L_1 L_3}{3}\frac{d^2\lambda_2}{dt^2}\delta\lambda_1 \tag{50}$$

$$\rho L_1 L_2 z^2 \frac{d^2\lambda_1}{dt^2}\delta\lambda_1 \int_0^{L_3} z^2 dx = \frac{L_3^3 \rho L_1 L_2}{3}\frac{d^2\lambda_3}{dt^2}\delta\lambda_1 \tag{51}$$

Based on the energy balance, the increase of the free energy of the DE membrane equals to the sum of the works done by the battery $\Phi\delta Q$, the tensile forces, the inertia forces and the environment temperature. Doing so gives,

$$\begin{aligned}L_1 L_2 L_3 \delta W = &\Phi\delta Q + P_1 L_1 \delta\lambda_1 + P_2 L_2 \delta\lambda_2 - \frac{L_1^3 \rho L_2 L_3}{3}\frac{d^2\lambda_1}{dt^2}\delta\lambda_1 \\ &- \frac{L_2^3 \rho L_1 L_3}{3}\frac{d^2\lambda_2}{dt^2}\delta\lambda_1 - \frac{L_3^3 \rho L_1 L_2}{3}\frac{d^2\lambda_3}{dt^2}\delta\lambda_1 - \rho L_1 L_2 L_3 k\delta T\end{aligned} \tag{52}$$

where W is the free energy density of the DE, k is the specific entropy of the DE,

$$\begin{aligned}\frac{d^2\lambda_3}{dt^2} = &-\lambda_1^{-2}\lambda_2^{-1}\frac{d^2\lambda_1}{dt^2} - \lambda_1^{-1}\lambda_2^{-2}\frac{d^2\lambda_2}{dt^2} + 2\lambda_1^{-3}\lambda_2^{-1}\left(\frac{d\lambda_1}{dt}\right)^2 \\ &+ 2\lambda_1^{-1}\lambda_2^{-3}\left(\frac{d\lambda_2}{dt}\right)^2 + 2\lambda_1^{-2}\lambda_2^{-2}\frac{d\lambda_1}{dt}\frac{d\lambda_2}{dt}\end{aligned} \tag{53}$$

$$\delta\lambda_3 = -\lambda_1^{-2}\lambda_2^{-1}\delta\lambda_1 - \lambda_1^{-1}\lambda_2^{-2}\delta\lambda_2 \tag{54}$$

Submitting Eq. (48) and Eq. (54) to Eq. (52) yields:

$$\begin{aligned}L_1L_2L_3\delta W = &\Phi\frac{\epsilon(\lambda_1,\lambda_2,T)\lambda_1^2\lambda_2^2}{L_3/L_1L_2}\delta\Phi + 2\Phi^2\frac{\varepsilon(\lambda_1,\lambda_2,T)\lambda_1\lambda_2^2}{L_3/L_1L_2}\delta\lambda_1 \\ &+ 2\Phi^2\frac{\varepsilon(\lambda_1,\lambda_2,T)\lambda_1^2\lambda_2}{L_3/L_1L_2}\delta\lambda_2 + \Phi^2\frac{\lambda_1^2\lambda_2^2}{L_3/L_1L_2}\frac{\partial\varepsilon(\lambda_1,\lambda_2,T)}{\partial\lambda_1}\delta\lambda_1 \\ &+ \Phi^2\frac{\lambda_1^2\lambda_2^2}{L_3/L_1L_2}\frac{\partial\varepsilon(\lambda_1,\lambda_2,T)}{\partial\lambda_2}\delta\lambda_2 + \Phi^2\frac{\lambda_1^2\lambda_2^2}{L_3/L_1L_2}\frac{\partial\varepsilon(\lambda_1,\lambda_2,T)}{\partial T}\delta T \\ &+ P_1L_1\delta\lambda_1 + P_2L_2\delta\lambda_2 - \frac{L_1^3\rho L_2L_3}{3}\frac{d^2\lambda_1}{dt^2}\delta\lambda_1 \\ &- \frac{L_2^3\rho L_1L_3}{3}\frac{d^2\lambda_2}{dt^2}\delta\lambda_1 + \frac{L_3^3\rho L_1L_2}{3}\frac{d^2\lambda_3}{dt^2}(\lambda_1^{-2}\lambda_2^{-1}\delta\lambda_1 + \lambda_1^{-1}\lambda_2^{-2}\delta\lambda_2)\end{aligned} \tag{55}$$

By solving Eq. (55), we have the following two equations as:

$$\begin{aligned}\frac{\partial W}{\partial\lambda_1} = &2\varepsilon(\lambda_1,\lambda_2,T)\left(\frac{\Phi}{L_3}\right)^2\lambda_1\lambda_2^2 \\ &+ \lambda_1^2\lambda_2^2\left(\frac{\Phi}{L_3}\right)^2\frac{\partial\varepsilon(\lambda_1,\lambda_2,T)}{\partial\lambda_1} \\ &+ \frac{P_1}{L_2L_3} - \frac{L_1^2\rho}{3}\frac{d^2\lambda_1}{dt^2} + \frac{L_3^2\rho}{3}\frac{d^2\lambda_3}{dt^2}\lambda_1^{-2}\lambda_2^{-1}\end{aligned} \tag{56}$$

$$\begin{aligned}\frac{\partial W}{\partial\lambda_2} = &2\varepsilon(\lambda_1,\lambda_2,T)\left(\frac{\Phi}{L_3}\right)^2\lambda_1^2\lambda_2 \\ &+ \lambda_1^2\lambda_2^2\left(\frac{\Phi}{L_3}\right)^2\frac{\partial\varepsilon(\lambda_1,\lambda_2,T)}{\partial\lambda_2} \\ &+ \frac{P_2}{L_1L_3} - \frac{L_2^2\rho}{3}\frac{d^2\lambda_2}{dt^2} + \frac{L_3^2\rho}{3}\frac{d^2\lambda_3}{dt^2}\lambda_1^{-1}\lambda_2^{-2}\end{aligned} \tag{57}$$

By substituting Eq. (44), Eq. (45) and (46) into Eq. (56), and (57) we can get:

$$\begin{aligned}\frac{L_1^2\rho}{3}\frac{d^2\lambda_1}{dt^2} = \frac{L_3^2\rho}{3}\frac{d^2\lambda_3}{dt^2}\lambda_1^{-2}\lambda_2^{-1} - \frac{\mu^{\alpha_0}(\lambda_1-\lambda_1^{-3}\lambda_2^{-2})}{1-\frac{\lambda_1^2+\lambda_2^2+\lambda_1^{-2}\lambda_2^{-2}-3}{J_{\lim}^{\alpha_0}}} \\ -\sum_{i=1}^{4}\frac{\mu^{\alpha_i}(\lambda_1\xi_{i1}^{-2}-\lambda_1^{-3}\lambda_2^{-2}\xi_{i1}^2\xi_{i2}^2)}{1-\frac{\lambda_1^2\xi_{i1}^{-2}+\lambda_2^2\xi_{i2}^{-2}+\lambda_1^{-2}\lambda_2^{-2}\xi_{i1}^2\xi_{i2}^2-3}{J_{\lim}^{\alpha_i}}} + \frac{P_1}{L_2L_3} \\ +\varepsilon(\lambda_1,\lambda_2,T)\left(\frac{\Phi}{L_3}\right)^2\lambda_1\lambda_2^2+\lambda_1^2\lambda_2^2\left(\frac{\Phi}{L_3}\right)^2\frac{\partial\varepsilon(\lambda_1,\lambda_2,T)}{\partial\lambda_1}\end{aligned} \tag{58}$$

$$\begin{aligned}\frac{L_2^2\rho}{3}\frac{d^2\lambda_2}{dt^2} = \frac{L_3^2\rho}{3}\frac{d^2\lambda_3}{dt^2}\lambda_1^{-1}\lambda_2^{-2} - \frac{\mu^{\alpha_0}(\lambda_2-\lambda_1^{-2}\lambda_2^{-3})}{1-\frac{\lambda_1^2+\lambda_2^2+\lambda_1^{-2}\lambda_2^{-2}-3}{J_{\lim}^{\alpha_0}}} \\ -\sum_{i=1}^{4}\frac{\mu^{\alpha_i}(\lambda_2\xi_{i2}^{-2}-\lambda_1^{-2}\lambda_2^{-3}\xi_{i1}^2\xi_{i2}^2)}{1-\frac{\lambda_1^2\xi_{i1}^{-2}+\lambda_2^2\xi_{i2}^{-2}+\lambda_1^{-2}\lambda_2^{-2}\xi_{i1}^2\xi_{i2}^2-3}{J_{\lim}^{\alpha_i}}} + \frac{P_2}{L_1L_3} \\ +\varepsilon(\lambda_1,\lambda_2,T)\left(\frac{\Phi}{L_3}\right)^2\lambda_1^2\lambda_2+\lambda_1^2\lambda_2^2\left(\frac{\Phi}{L_3}\right)^2\frac{\partial\varepsilon(\lambda_1,\lambda_2,T)}{\partial\lambda_2}\end{aligned} \tag{59}$$

The stress of the spring α_i $(i = 1, 2, 3, 4)$ is equal to the stress of the dashpot, which leads to $\partial W_{ela}^{\alpha_i}/\partial\xi_{ij} = \eta_i d\xi_{ij}/dt$, where $(j = 1, 2)$.

So the relationship between the stretches λ_1, λ_2 and the inelastic stretches ξ_{i1}, ξ_{i2} is defined as follows:

$$\frac{d\xi_{i1}}{dt} = \frac{\mu^{\alpha_i}}{6\eta_i}\frac{2\lambda_1^2\xi_{i1}^{-1}-\lambda_2^2\xi_{i1}\xi_{i2}^{-2}-\lambda_1^{-2}\lambda_2^{-2}\xi_{i1}^3\xi_{i2}^2}{1-\frac{\lambda_1^2\xi_{i1}^{-2}+\lambda_2^2\xi_{i2}^{-2}+\lambda_1^{-2}\lambda_2^{-2}\xi_{i1}^2\xi_{i2}^2-3}{J_{\lim}^{\alpha_i}}} \tag{60}$$

$$\frac{d\xi_{i2}}{dt} = \frac{\mu^{\alpha_i}}{6\eta_i}\frac{2\lambda_2^2\xi_{i2}^{-1}-\lambda_1^2\xi_{i1}^{-2}\xi_{i2}-\lambda_1^{-2}\lambda_2^{-2}\xi_{i1}^2\xi_{i2}^3}{1-\frac{\lambda_1^2\xi_{i1}^{-2}+\lambda_2^2\xi_{i2}^{-2}+\lambda_1^{-2}\lambda_2^{-2}\xi_{i1}^2\xi_{i2}^2-3}{J_{\lim}^{\alpha_i}}} \tag{61}$$

The relaxation time of the DE $\tau(t)$ can be expressed as $\tau_i(t) = \eta_i/\mu^{\alpha_i}$.

Submitting Eq. (53) into Eq. (58) and Eq. (59) yields:

$$\begin{aligned}\frac{L_1^2\rho}{3}\frac{d^2\lambda_1}{dt^2} = &-\frac{L_3^2\rho}{3}\frac{d^2\lambda_3}{dt^2}\lambda_1^{-4}\lambda_2^{-2} - \frac{L_3^2\rho}{3}\frac{d^2\lambda_2}{dt^2}\lambda_1^{-3}\lambda_2^{-3} \\ &+ \frac{2L_3^2\rho}{3}\left(\frac{d\lambda_1}{dt}\right)^2\lambda_1^{-5}\lambda_2^{-2} + \frac{2L_3^2\rho}{3}\left(\frac{d\lambda_2}{dt}\right)^2\lambda_1^{-3}\lambda_2^{-4} \\ &+ \frac{2L_3^2\rho}{3}\frac{d\lambda_1}{dt}\frac{d\lambda_2}{dt}\lambda_1^{-4}\lambda_2^{-3} - \frac{\mu^{\alpha_0}(\lambda_1 - \lambda_1^{-3}\lambda_2^{-2})}{1 - \frac{\lambda_1^2+\lambda_2^2+\lambda_1^{-2}\lambda_2^{-2}-3}{J_{\lim}^{\alpha_0}}} \\ &- \sum_{i=1}^{4}\frac{\mu^{\alpha_i}(\lambda_1\xi_{i1}^{-2} - \lambda_1^{-3}\lambda_2^{-2}\xi_{i1}^2\xi_{i2}^2)}{1 - \frac{\lambda_1^2\xi_{i1}^{-2}+\lambda_2^2\xi_{i2}^{-2}+\lambda_1^{-2}\lambda_2^{-2}\xi_{i1}^2\xi_{i2}^2-3}{J_{\lim}^{\alpha_i}}} + \frac{P_1}{L_2L_3} \\ &+ \varepsilon(\lambda_1,\lambda_2,T)\left(\frac{\Phi}{L_3}\right)^2\lambda_1\lambda_2^2 + \lambda_1^2\lambda_2^2\left(\frac{\Phi}{L_3}\right)^2\frac{\partial\varepsilon(\lambda_1,\lambda_2,T)}{\partial\lambda_1}\end{aligned} \tag{62}$$

$$\begin{aligned}\frac{L_2^2\rho}{3}\frac{d^2\lambda_2}{dt^2} = &-\frac{L_3^2\rho}{3}\frac{d^2\lambda_3}{dt^2}\lambda_1^{-3}\lambda_2^{-3} - \frac{L_3^2\rho}{3}\frac{d^2\lambda_2}{dt^2}\lambda_1^{-2}\lambda_2^{-4} \\ &+ \frac{2L_3^2\rho}{3}\left(\frac{d\lambda_1}{dt}\right)^2\lambda_1^{-4}\lambda_2^{-3} + \frac{2L_3^2\rho}{3}\left(\frac{d\lambda_2}{dt}\right)^2\lambda_1^{-2}\lambda_2^{-5} \\ &+ \frac{2L_3^2\rho}{3}\frac{d\lambda_1}{dt}\frac{d\lambda_2}{dt}\lambda_1^{-3}\lambda_2^{-4} - \frac{\mu^{\alpha_0}(\lambda_2 - \lambda_1^{-2}\lambda_2^{-3})}{1 - \frac{\lambda_1^2+\lambda_2^2+\lambda_1^{-2}\lambda_2^{-2}-3}{J_{\lim}^{\alpha_0}}} \\ &- \sum_{i=1}^{4}\frac{\mu^{\alpha_i}(\lambda_2\xi_{i2}^{-2} - \lambda_1^{-2}\lambda_2^{-3}\xi_{i1}^2\xi_{i2}^2)}{1 - \frac{\lambda_1^2\xi_{i1}^{-2}+\lambda_2^2\xi_{i2}^{-2}+\lambda_1^{-2}\lambda_2^{-2}\xi_{i1}^2\xi_{i2}^2-3}{J_{\lim}^{\alpha_i}}} + \frac{P_2}{L_1L_3} \\ &+ \varepsilon(\lambda_1,\lambda_2,T)\left(\frac{\Phi}{L_3}\right)^2\lambda_1^2\lambda_2 + \lambda_1^2\lambda_2^2\left(\frac{\Phi}{L_3}\right)^2\frac{\partial\varepsilon(\lambda_1,\lambda_2,T)}{\partial\lambda_2}\end{aligned} \tag{63}$$

The dynamic model of the DE with the rectangle shape can be obtained by combing eq. (60), (61) and Eq. (62), (63). In this study, we assume that the membrane of the DE is subjected to a homogeneous, equal-biaxial force $P_1 = P_2 = P$ and equal dimensions $L_1 = L_2 = L$. Furthermore, since we assume that DE is isotropic, the elastomer would be subject to equal biaxial stresses $s_1 = s_2 = s$, so that the two in-plane stretches are equal, which we denote as $\lambda_1 = \lambda_2 = \lambda$, $\xi_{i1} = \xi_{i2} = \xi$, and consequently we can receive the dynamic model of the DE as:

$$\left(\frac{L^2\rho}{3}+\frac{2L_3^2\rho}{3}\lambda^{-6}\right)\ddot{\lambda}=2L_3^2\rho\left(\dot{\lambda}\right)^2\lambda^{-7}-\frac{\mu^{\alpha_0}(\lambda-\lambda^{-5})}{1-\frac{2\lambda^2+\lambda^{-4}-3}{J_{\lim}^{\alpha_0}}}$$
$$-\sum_{i=1}^{4}\frac{\mu^{\alpha_i}(\lambda\xi^{-2}-\lambda^{-5}\xi^4)}{1-\frac{2\lambda^2\xi^{-2}+\lambda^{-4}\xi^4-3}{J_{\lim}^{\alpha_i}}}+\frac{P}{LL_3} \tag{64}$$
$$+\left[\frac{\varepsilon(\lambda,T)\lambda^3+\lambda^4\partial\varepsilon(\lambda,T)/\partial\lambda}{L_3^2}\right]\Phi^2$$

$$\dot{\xi}_i=\frac{\mu^{\alpha_i}}{6\eta_i}\frac{\lambda^2\xi^{-1}-\lambda^{-4}\xi^5}{1-\frac{2\lambda^2\xi^{-2}+\lambda^{-4}\xi^4-3}{J_{\lim}^{\alpha_i}}} \tag{65}$$

According to (Chen, Deng, He, Li, & Li, 2016), $\varepsilon=(\lambda,T)$ can be expressed as follows:

$$\varepsilon(\lambda,T)=\varepsilon_0+\Delta\varepsilon \tag{66}$$

where $\varepsilon_0=\frac{b_\varepsilon}{T_0}+c_\varepsilon$ is a constant value, which represents the initial permittivity of the DE, and $\Delta\varepsilon=\frac{a_\varepsilon\lambda^2+b_\varepsilon(T_0-T)}{(T_0T)}$ represents the change of the permittivity of the DE caused by the deformation of the DE and the change of the environment temperature; $a_\varepsilon, b_\varepsilon, and c_\varepsilon$ have constant values. Therefore, $\frac{\partial\varepsilon(\lambda,T)}{\partial\lambda}$ can be written as:

$$\frac{\partial\varepsilon(\lambda,T)}{\partial\lambda}=2a_\varepsilon\lambda \tag{67}$$

By substituting Eq. (66), and Eq. (67) into Eq. (64), we can finally get:

$$\left(\frac{L^2\rho}{3}+\frac{2L_3^2\rho}{3}\lambda^{-6}\right)\ddot{\lambda}=2L_3^2\rho\left(\dot{\lambda}\right)^2\lambda^{-7}-\frac{\mu^{\alpha_0}(\lambda-\lambda^{-5})}{1-\frac{2\lambda^2+\lambda^{-4}-3}{J_{\lim}^{\alpha_0}}}$$
$$-\sum_{i=1}^{4}\frac{\mu^{\alpha_i}(\lambda\xi^{-2}-\lambda^{-5}\xi^4)}{1-\frac{2\lambda^2\xi^{-2}+\lambda^{-4}\xi^4-3}{J_{\lim}^{\alpha_i}}}+\frac{P}{LL_3} \tag{68}$$
$$+\frac{\varepsilon_0\lambda^3}{L_3^2}\Phi^2+\frac{\Delta\lambda^3+2a_\varepsilon\lambda^5}{L_3^2}\Phi^2$$

In Eq. (68) $\frac{\varepsilon_0\lambda^3}{L_3^2}\Phi^2$ can be regarded as the contribution of the Maxwell force, and $\frac{\Delta\lambda^3+2a_\varepsilon\lambda^5}{L_3^2}\Phi^2$ can be regarded as the contribution of the electrostrictive force. Thus, both the Maxwell force and the electrostrictive force are considered in the modeling of the DE.

Chapter 4

Experimental Implementation and Model Verifications

4.1 Experimental Implementation

4.1.1 Experimental Setup

The experiment was done on a square dielectric elastomer actuator made of VHB 4910 attached to a rigid frame, and electrodes made with carbon grease.

- **First:**

  The DE membrane is prestretched onto a square rigid frame made of acrylic with dimensions of $14cm$ outer length and $11.5cm$ Inner length. The membrane is stretched two times equally in all directions. Thus, the dimension ratio of the acrylic frame and the VHB film is $(2:1)$. So in this case, the VHB is cut with a square shape of a length $5.75cm$. Then, the whole VHB membrane is attached to the rigid frame equally.

- **Second:**

  In the middle of the DE membrane, an area of a square shape with $3cm$ length was painted with carbon grease on the both sides of the membrane, and the both sides are matched perfectly to ensure the electrical conductivity.

- **Third:**

  Short pieces of copper tape with around 4” in length and $1/2$” width are attached on opposing sides of the active area, and a line of carbon grease was drawn from one active area to a piece of copper tape, and another line from the opposing side.

- **Finally:**

  The high voltage amplifier is connected to the pieces of copper tape on the two sides of DE film.

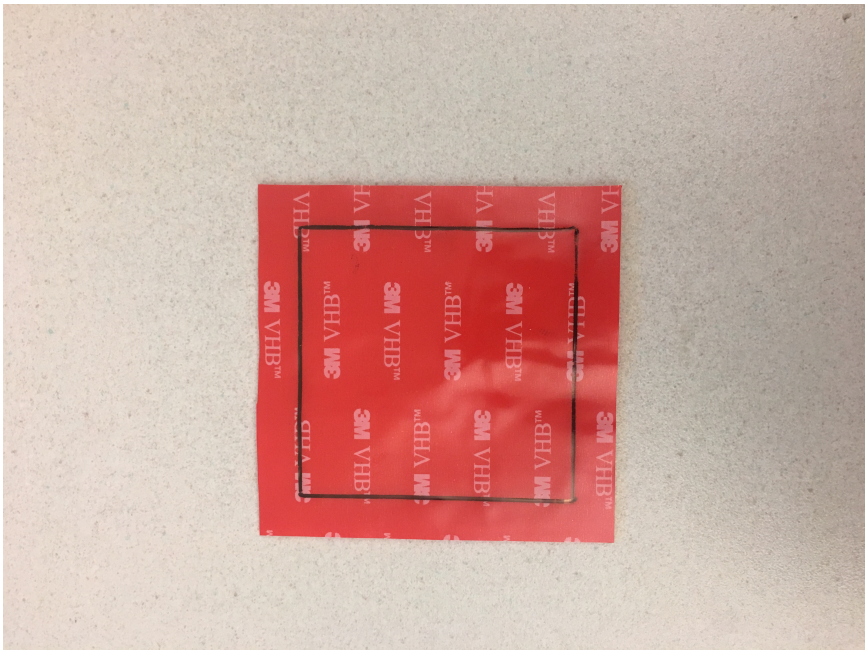

Figure 4.1: Step 1.

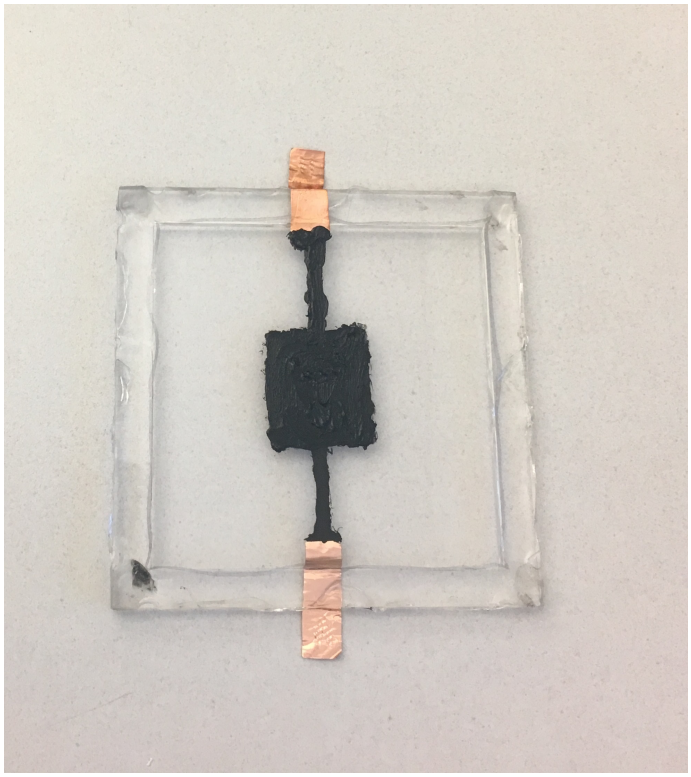

Figure 4.2: Step 2.

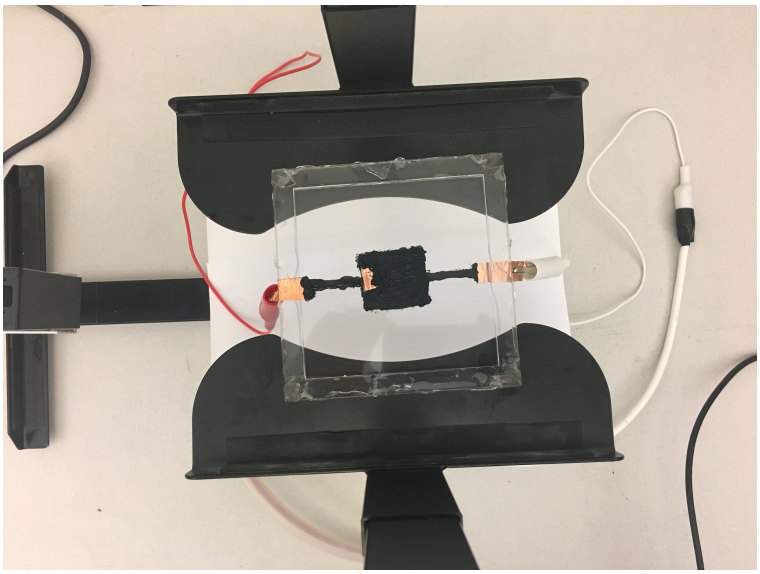

Figure 4.3: Step 3.

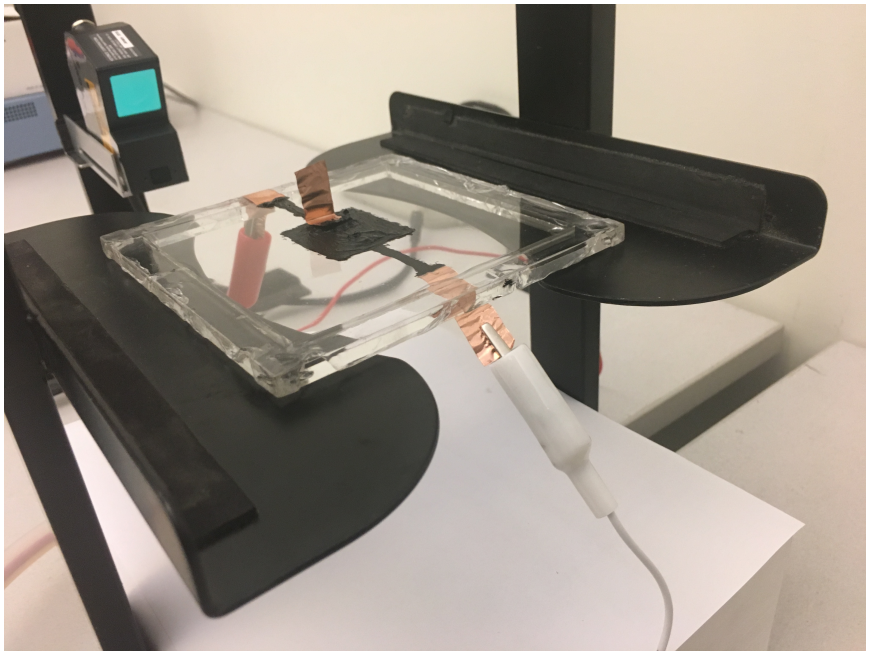

Figure 4.4: Step 4.

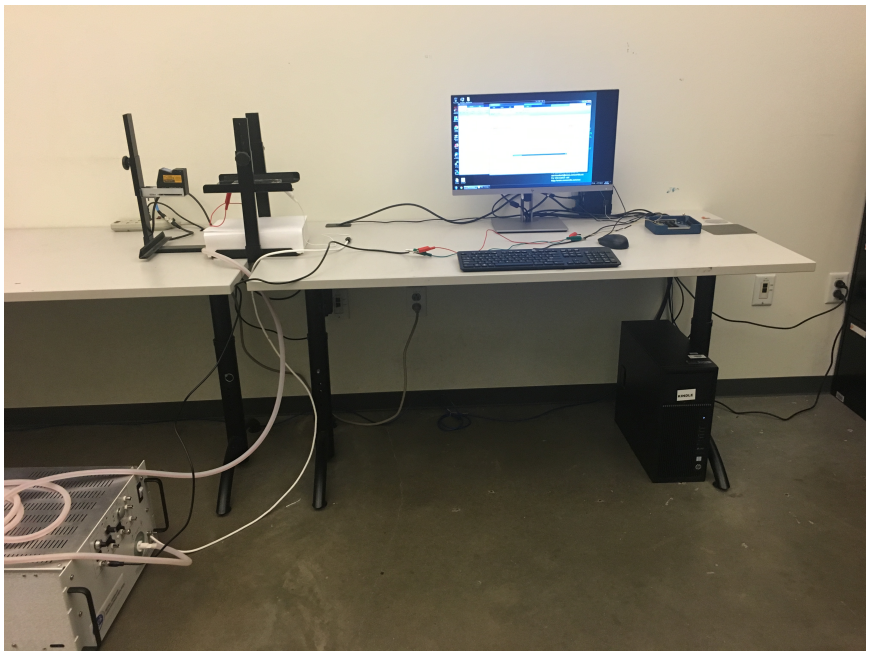

Figure 4.5: The Whole Setup.

4.1.2 Materials Used

- **3M VHB 4910 FOAM TAPE:**

  The DE film used in this experiment is 3M VHB 4910 Foam Tape from an American company called McMaster-Carr. The Material is Adhesive on Both Sides, with 12" Width x 1 Yard Length, .040" Thick. VHB 4910 is a well-known material in the field of soft robotics and its application due to the features it has such as high energy density, low mass density, high tensile strength, and good ability to operate at a good range of temperature from $-10°$C to $90°$C.

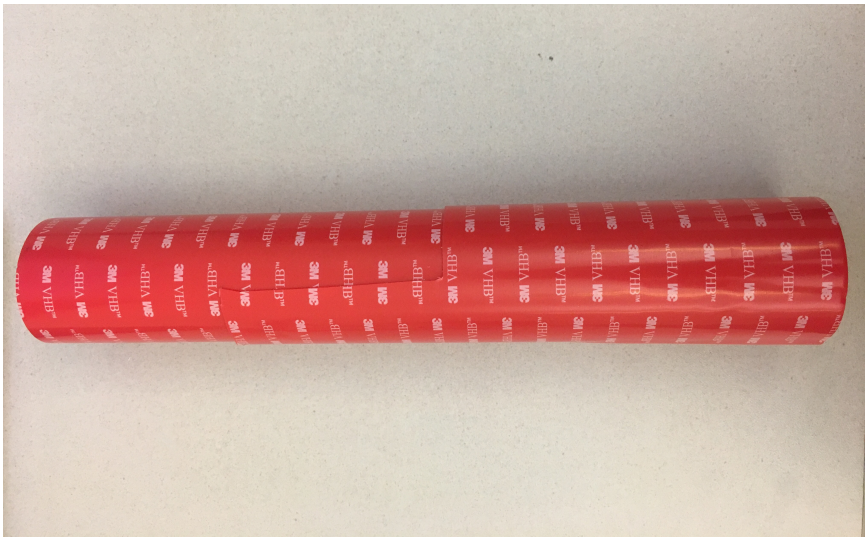

Figure 4.6: 3M VHB 4910 Foam Tape.

- **HIGH-VOLTAGE POWER AMPLIFIER:**

  The model used in this experiment is $10/40A - HS$ from TREK Inc, which is a company from USA. The device is a DC-stable, high-voltage power amplifier. It can provide a precision range of voltages from 0 to 10 kV DC, a range of output current from 0 to 40 mA DC with peak AC, and 120 mA peak AC for 1 ms (not more than 40 mA rms).

Figure 4.7: High-Voltage Power Amplifier.

- **CARBON GREASE:** It is made of silicon oil loaded with branched carbon to produce and improve electrical connections. It is designed to operate in a wide range of temperatures from $-68°$C to $200°$C, and with a volume resistivity of $117cm$.

Figure 4.8: Carbon Grease.

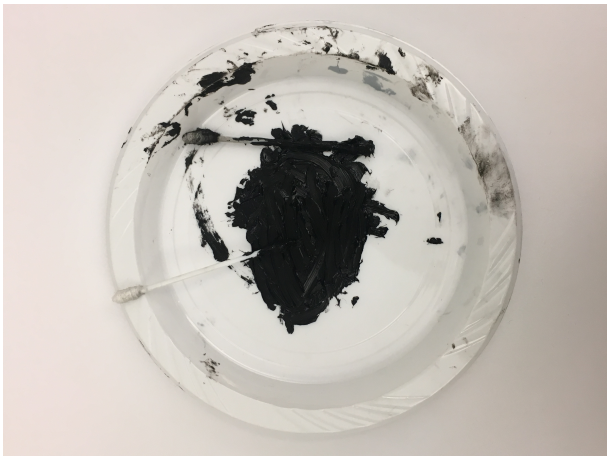

Figure 4.9: Carbon Grease.

- **COPPER TAPE:**

  It is a highly conductive copper electrical tape with 1" width and $18ft.$ length. It is an adhesive acrylic tape, and the temperature range that can be produced on is from $-40°$C to $325°$F.

[H] 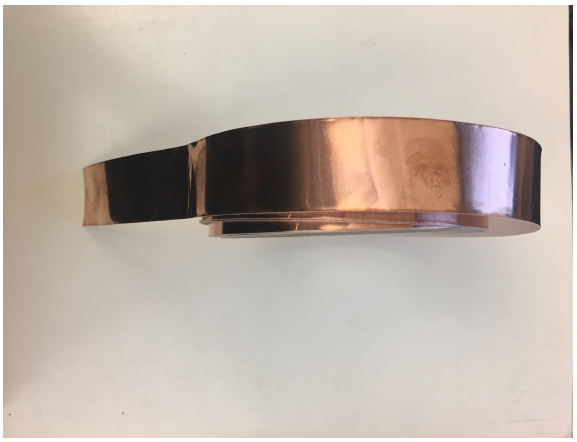

Figure 4.10: Copper Tape.

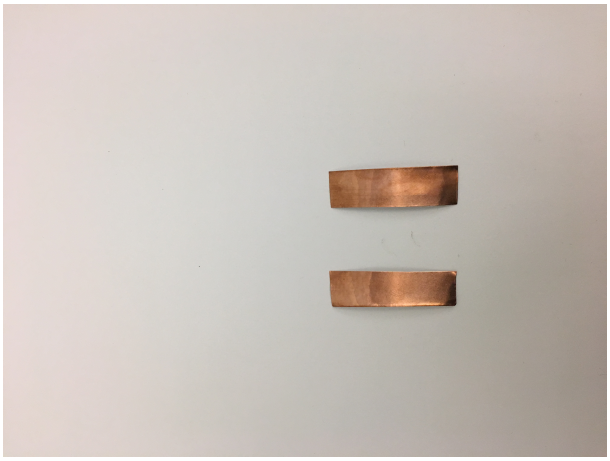

Figure 4.11: Two Pieces of Copper Tape.

- **LASER DISPLACEMENT SENSOR:**

  It's model is LK-H152, and it is provided by a Japanese company called Keyence company. Laser displacement sensors are designed with high speed and accuracy. They can provide excellent performance in detecting the displacement measurements undergoing high voltage power.

Figure 4.12: Laser Displacement Sensor.

4.2 Model Identifications

By using MATLAB, simulation studies for the proposed DE model are done with different patterns of voltages, frequencies, and temperatures. The model is then verified by doing an experiment, and the experimental results are matched with the simulations as will be presented in the next section. In order to find the required parameters (μ, J_{lim}, η) in equations (65) and (68), the Differential Evolution algorithm is used, and the software used in this study to implement the algorithms is MATLAB/Simulink.

In recent years, Differential Evolution has become important and necessary metaheuristics in fields such as engineering, statistics and finance. It was first introduced by Storn and Price in 1995

(Storn & Price, 1995). Differential Evolution is used to obtain attractive results in solving many optimization problems. It is difficult if not impossible to solve analytically certain problems; for example, the problems that are flat, noisy, constrictive, non-linear, non-continuous, non- differentiable, multi-dimensional or have many local minima. Thus, Differential Evolution is designed to solve such problems practically by finding the approximate solutions, optimising real parameters, and real valued functions. Differential Evolution algorithm is a population-based algorithm such as genetic algorithms using similar operators; crossover, mutation and selection.

Differential Evolution algorithm has the advantage of obtaining the true global minimum regardless of the initial parameter value, using few control parameters, and fast convergence.

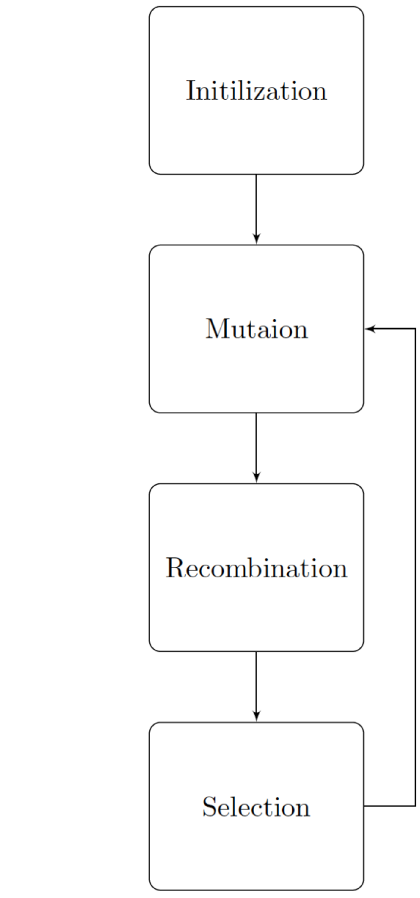

Figure 4.13: Basic steps of an Differential Evolution Algorithm.

The initialization used for the simulations are listed in the table below:

Table 4.1: Model Initialization

.

Model Initialization	
Time T_s	$20s$
Initial State of units (A, B, C, D, E) X_0	$[2, 2, 2, 2, 2]$
Initial Velocity V_0	0
DE dimension (L)	$0.03m$
DE thickness (L_3)	$0.001m$
Density (ρ)	$960J/m^3$
The permittivity of DE (ε_0)	$8.85418 * 10^{-12}Fm^{-1}$
Population Size	50
NO. of initialized Max. and Min. bounds	14
Maximum number of Iterations (G)	100
Mutation Factor (F)	0.6
Crossover Rate (cr)	0.9

As a part of the initialization step, the range of the values (maximum and minimum) of the required parameters (μ, J_{lim}, η) should be defined.

The maximum and minimum values of the shear modulus (μ) and the limiting stretch (J_{lim}) are classified in the table below:

Table 4.2: Upper and lower bounds for (μ, J_{lim})

Parameters (μ, J_{lim})		
Unit	μ	J_{lim}
0	$Min = 0.01; Max = 500$	$Min = 100; Max = 400$
1	$Min = 0.01; Max = 500$	$Min = 200; Max = 500$
2	$Min = 0.01; Max = 500$	$Min = 300; Max = 600$
3	$Min = 0.01; Max = 500$	$Min = 400; Max = 700$
4	$Min = 0.01; Max = 500$	$Min = 500; Max = 800$

The maximum and minimum values of the parameter (η) is classified in the table below:

Table 4.3: Upper and lower bounds for (η)

Parameter (η)	
Unit	η
1	$Min = 1 * 10^{-5}; Max = 20$
2	$Min = 1 * 10^{-5}; Max = 20$
3	$Min = 1 * 10^{-5}; Max = 20$
4	$Min = 1 * 10^{-5}; Max = 20$

The evolution function of the Differential Evolution algorithm used for this model is as follows:

$e = \sum_{i=1}^{end} \mid X_i - X_{id} \mid$

The program flow of the DE algorithm is as follows:

- **Step 1:**

  Randomly initialize the assumed target values of (μ, J_{lim}, η).

- **Step 2:**

  Calculate the evolution function $\left(e = \sum_{i=1}^{end} \mid X_i - X_{id} \mid\right)$, where X_i refers to the simulation results on a specific time, and X_{id} is the experiment results on the corresponding time. By substituting the simulation values X_i from the experiment values X_{id} for each assumed value and doing that repeatedly until the target is accomplished, which means we find the correct values for the required parameters (μ, J_{lim}, η).

- **Step 3:**

  If the evolution function (e) is less than (0.01), we obtain the fitting values of (μ, J_{lim}, η). Otherwise, the program continues to the next step.

- **Step 4:**

  Update the assumed values of the required parameters (μ, J_{lim}, η) by mutation, crossover, and selection operations with the mutation rate (pm) and crossover rate (pc). Then, the program jumps to Step 2.

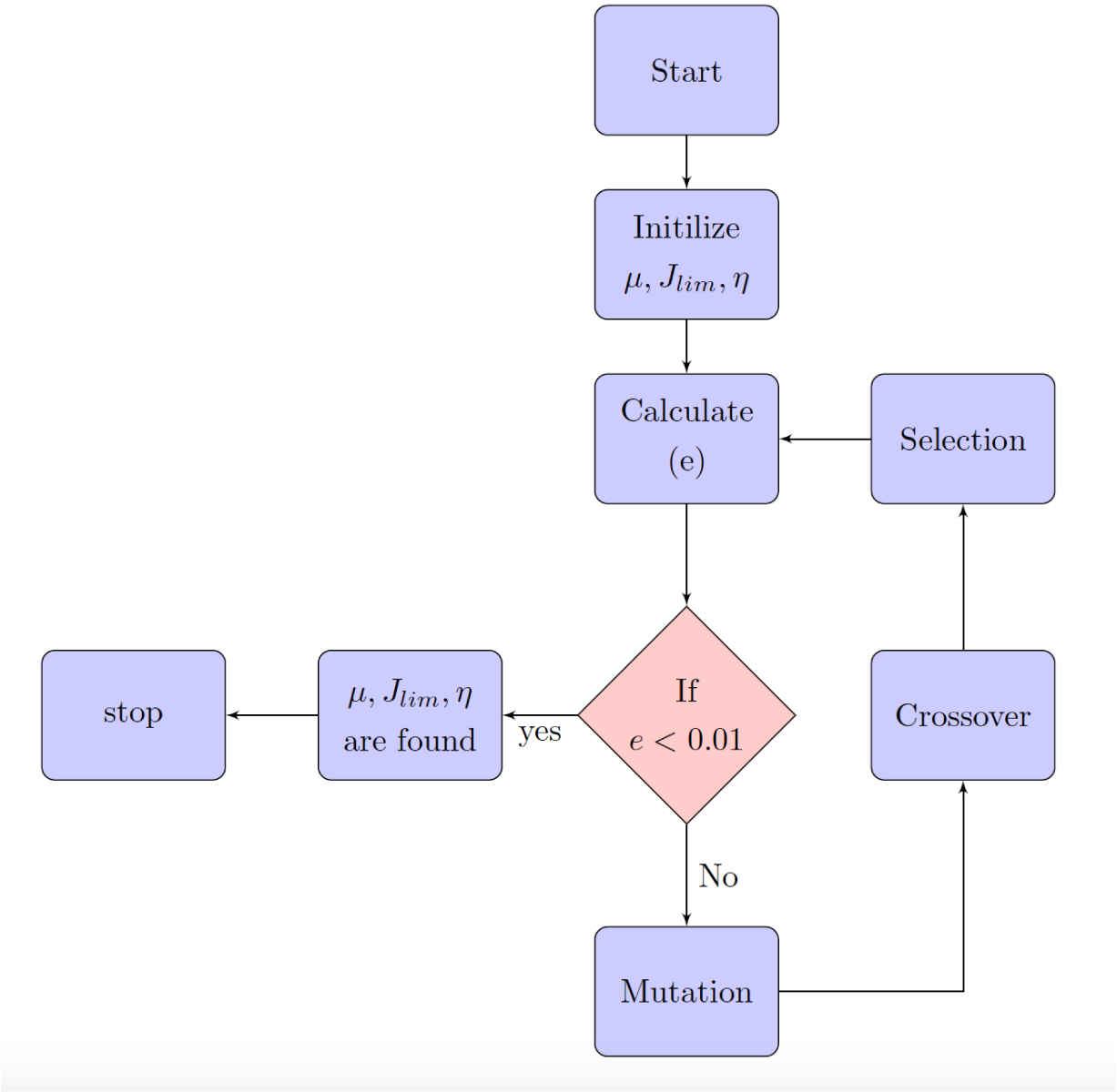

Figure 4.14: The Differential Evolution algorithm process for the proposed model.

The values of required model parameters (μ, J_{lim}, η) are listed in the table below:

Table 4.4: Results Verifications

Model Parameters			
Unit	μ	J_{lim}	η
0	$6.54472 * 10^4$	$3.51629 * 10^2$	No dashpot
1	$1.23636 * 10^5$	$4.00619 * 10^2$	$1.10671 * 10^4$
2	$3.08529 * 10^4$	$4.32838 * 10^2$	$1.54164 * 10^5$
3	$4.99622 * 10^5$	$4.05422 * 10^2$	4.99622
4	$3.98081 * 10^5$	$7.95496 * 10^2$	$2.68992 * 10^4$

4.3 Model Verifications

Based on the real experimental results, the dynamic behavior of the DE was simulated with MATLAB under a wide range of conditions to see how it behaves. The real parameters found from the experiment were used in the Differential Evolution algorithm to find the appropriate values of the required parameters (μ, J_{lim}, η), as mentioned in section (4.2), and then the the simulations were done under three different sets of voltages, frequencies, and temperatures.

- **First Set:**

  For the first test, the simulation was applied for four different voltage levels, which are $(5000V, 6000V, 7000V, 8000V)$. In this set, the frequency and the temperature remains unchanged. The results of the first set of simulations can bee seen from figures (4.17 and 4.18)

- **Second Set:**

  For the second set, the simulation was applied for four different frequencies levels, which are $(1/3Hz, 1/6Hz, 1/9Hz, 1/12Hz)$. In this set, the voltage and the temperature remains unchanged. The results of the second set of simulations can bee seen from figures (4.19 and 4.20)

- **Third Set:**

  For the second set, the simulation was applied for four different temperatures levels, which are $(266k, 296k, 306k, 316k)$. In this set, the voltage and the frequency remains unchanged. The results of the third set of simulations can bee seen from figures (4.21 and 4.22)

The experiment was conducted under set of voltage, frequency, and temperature. The comparison between the simulation results and experimental results are closely related and show a good agreement, which can determine the validity of the model. The comparison between the simulation and experiment are shown in the figures below:

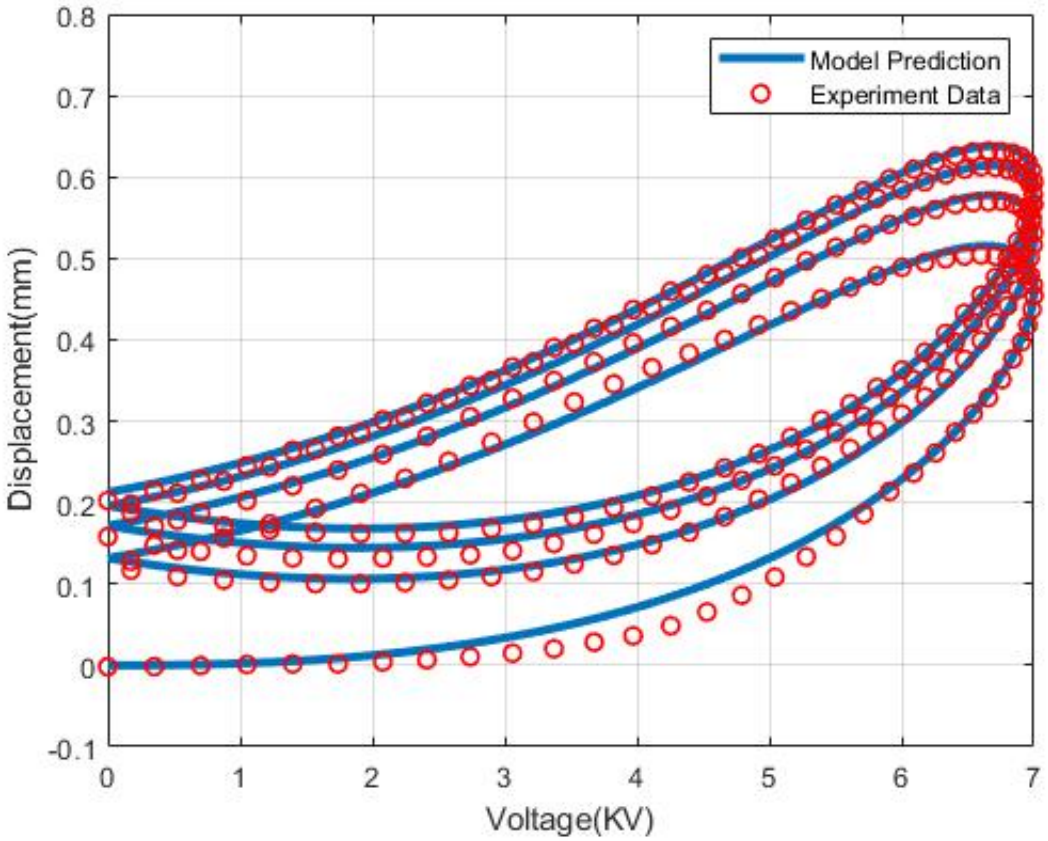

Figure 4.15: Displacement as a function of voltage for the first four cycles.

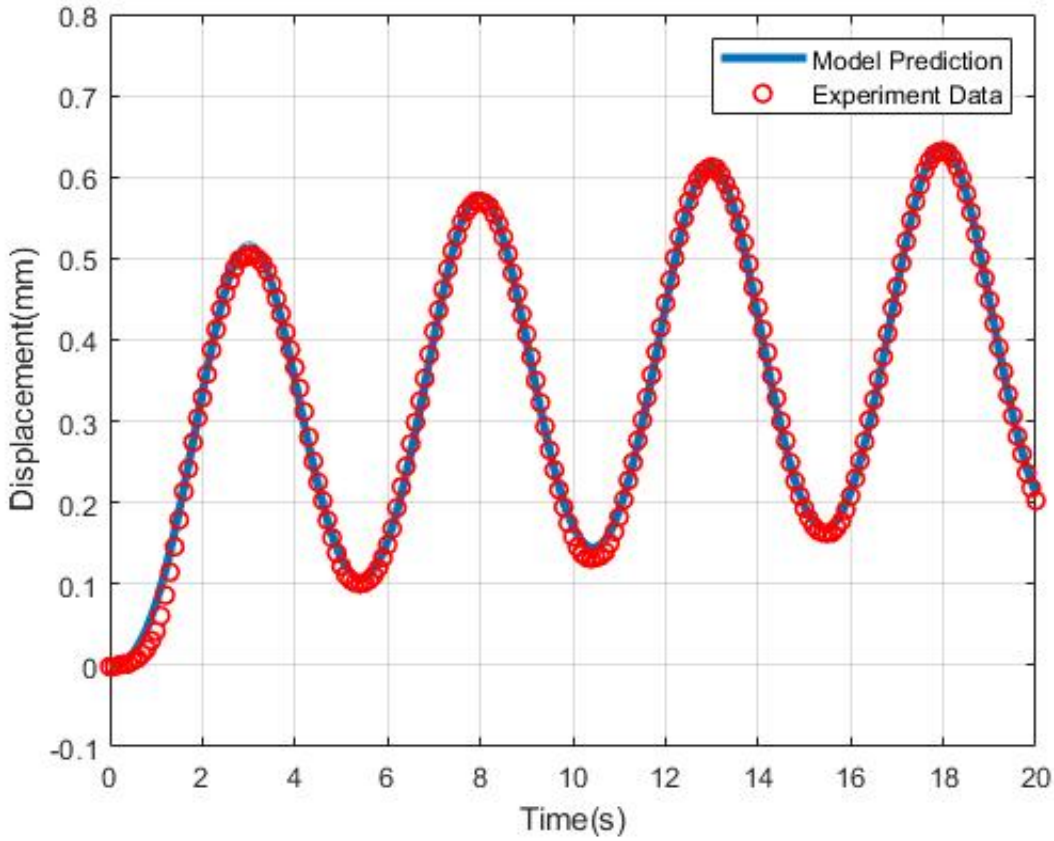

Figure 4.16: Displacement as a function of time for the first four cycles.

The experiment and model responses are conducted for the model shown in figure (3.3). It can be seen from the figures above (4.15) and (4.16) show the effectiveness of the proposed model, where the blue curves represent the model prediction, while the red circles represent the experimental results. Figure (4.15) shows the displacement as a function of voltage for the first four cycles while figure (4.16) represents the displacement as a function of time for the first four cycles.

As it is shown, there is a good agreement between the model prediction and experimental data. We can see from figure (4.15) that the creep can be predicted by the model, which figure (4.16) can verify that. The values of the different material parameters are given as shown in table (4.2). The time to complete the four cycles is 20 seconds.

The relaxation time is as follows:

- For (α_1) the relaxation time is ($T_1 = 0.08951s$).
- For (α_2) the relaxation time is ($T_2 = 4.99616s$).
- For (α_3) the relaxation time is ($T_3 = 1 * 10^{-5}s$).
- For (α_4) the relaxation time is ($T_4 = 0.06757s$).

The experimental test was conducted at room temperature ($T = 296K$), under frequency $\left(\frac{1}{9}Hz\right)$, and the voltage used is ($V = 7000V$). From the figures (4.15) and (4.16), we can see that the frequency does not change during the cycles. Also, It can be seen that there is an error at the first cycle; however, the predicted root-mean-squared error between the model prediction and the experimental response is very small.

4.4 Results and Discussion

In this section, the model verifications are explained in details. There are four different voltage levels tested in this simulation, which are ($5000V, 6000V, 7000V, 8000V$). (4.17) illustrates the displacement versus voltage for different voltages. The blue line indicates the displacement under the voltage ($5000V$); it is clear that the displacement is very small. The orange line indicates how the displacement changes under the voltage ($6000V$) while the yellow line indicates the displacement change under the voltage ($7000V$). The purple line indicates the change of displacement under the voltage ($8000V$). From the figure (4.17), it can be concluded that when the voltage increases the displacement increases too. Figure (4.18) shows the displacement versus time for different voltages ($5000V, 6000V, 7000V, 8000V$). The time in the simulation was set for 20 seconds. This figure verifies the previous analysis, which is when the voltage becomes bigger, the amount of displacement becomes bigger. Also, it can be clearly seen that the frequency remains the same during the time.

In the model verification, four different frequencies were used, which are ($1/3Hz, 1/6Hz, 1/9Hz$, $1/12Hz$). Figure (4.19) shows the displacement versus voltage for different frequencies. The blue

line represents the displacement under the frequency $(1/3Hz)$. The orange line represents the displacement change under the frequency $(1/6Hz)$ while the yellow line indicates the displacement under the frequency $(1/9Hz)$. The purple line represents the amount of change in the displacement under the frequency $(1/12Hz)$. Figure (4.20) shows the displacement versus time for the same set of frequencies. During the 20 seconds, the frequency $(1/3Hz)$ remains the same. For the frequency $(1/6Hz)$, the frequency increases as well as the displacement. The displacement also increases under the frequency $(1/9Hz)$. The last frequency $(1/12Hz)$ show the bigger displacement of all the rest of frequencies. According to the analysis of the figures (4.19) and (4.20), the displacement gets biggest when the frequency gets smaller. Moreover, the change of the frequency is very slow when the frequency is low.

Four different temperatures were applied in the model verification, which are $(266k, 296k, 306k, 316k)$. Figure (4.21) shows the displacement versus voltage for different temperatures. The blue line refers to the displacement under the temperature $(266k)$. The orange line indicates how the displacement varies under the temperature $(296k)$. The yellow line represents the displacement change under the temperature $(306k)$. The purple line indicates the change of displacement under the temperature $(316k)$. Figure (4.22) shows the displacement versus time for the same values of temperatures. It can be seen that the frequency of the four cycles does not change during the time for each temperature. Furthermore, it can be seen that when the temperature goes up, the displacement goes down; so the displacement is inversely proportional to the temperature.

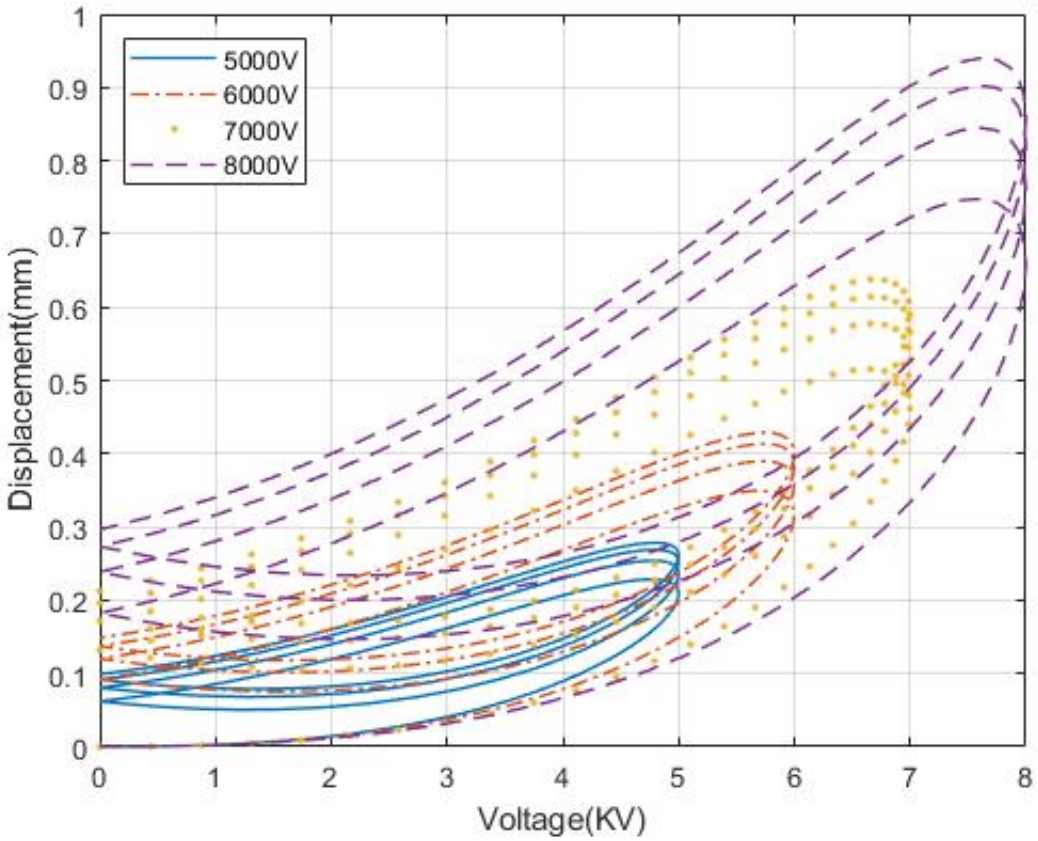

Figure 4.17: Displacement versus voltage for different voltages.

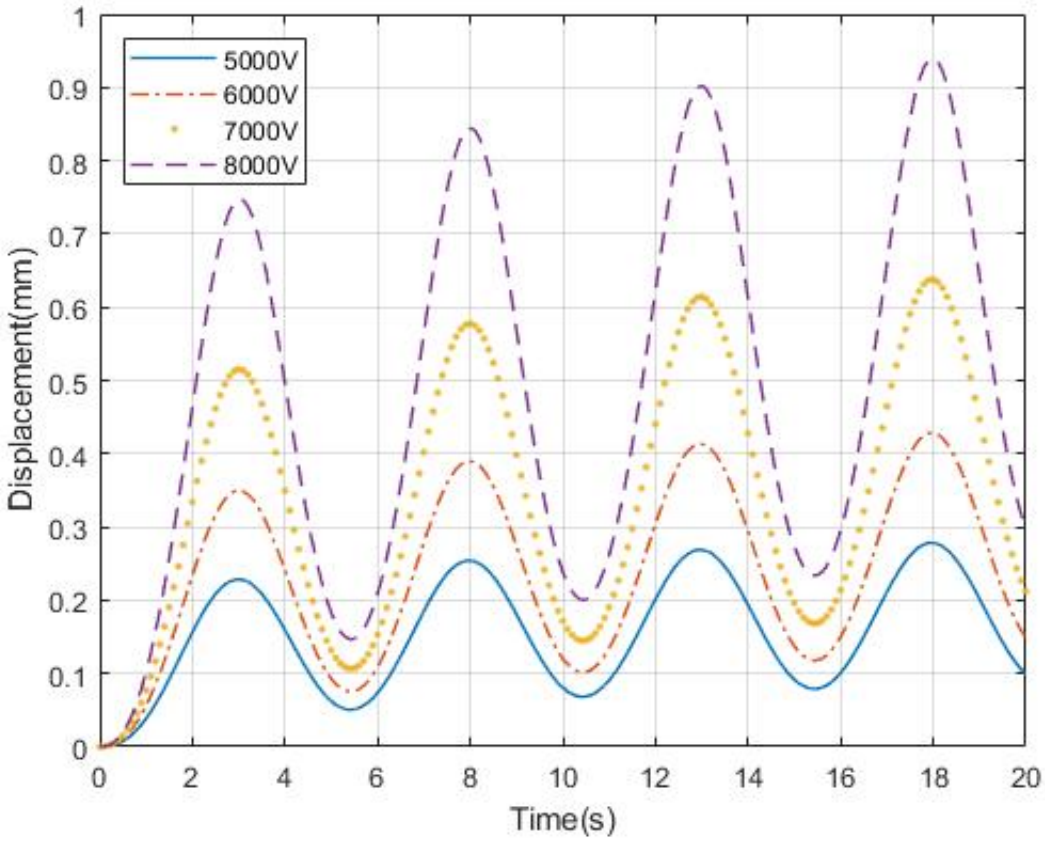

Figure 4.18: Displacement versus time for different voltages.

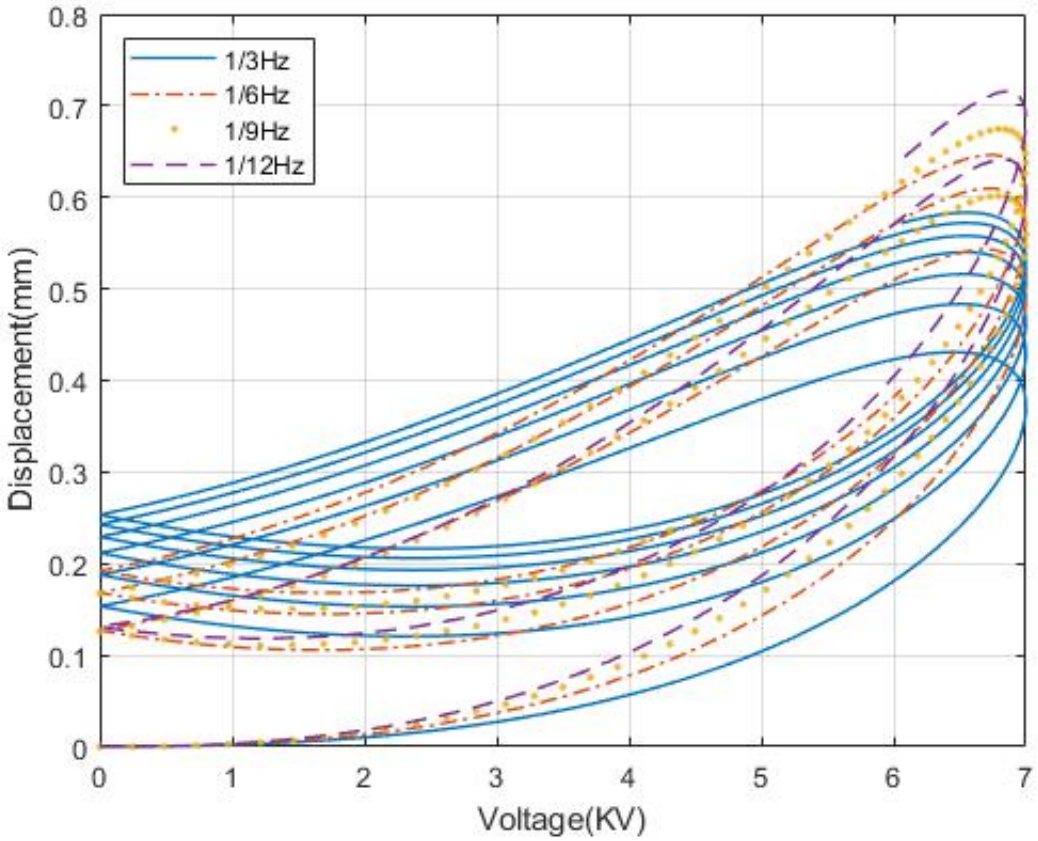

Figure 4.19: Displacement versus voltage for different frequencies.

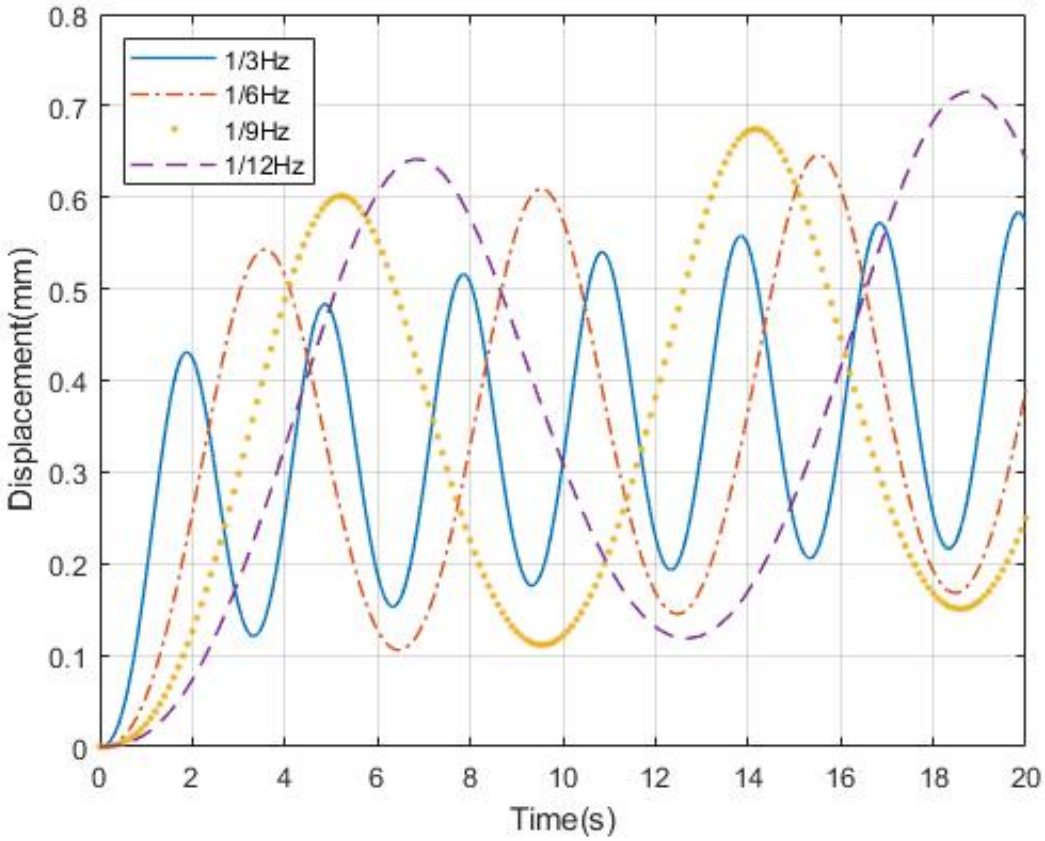

Figure 4.20: Displacement versus time for different frequencies.

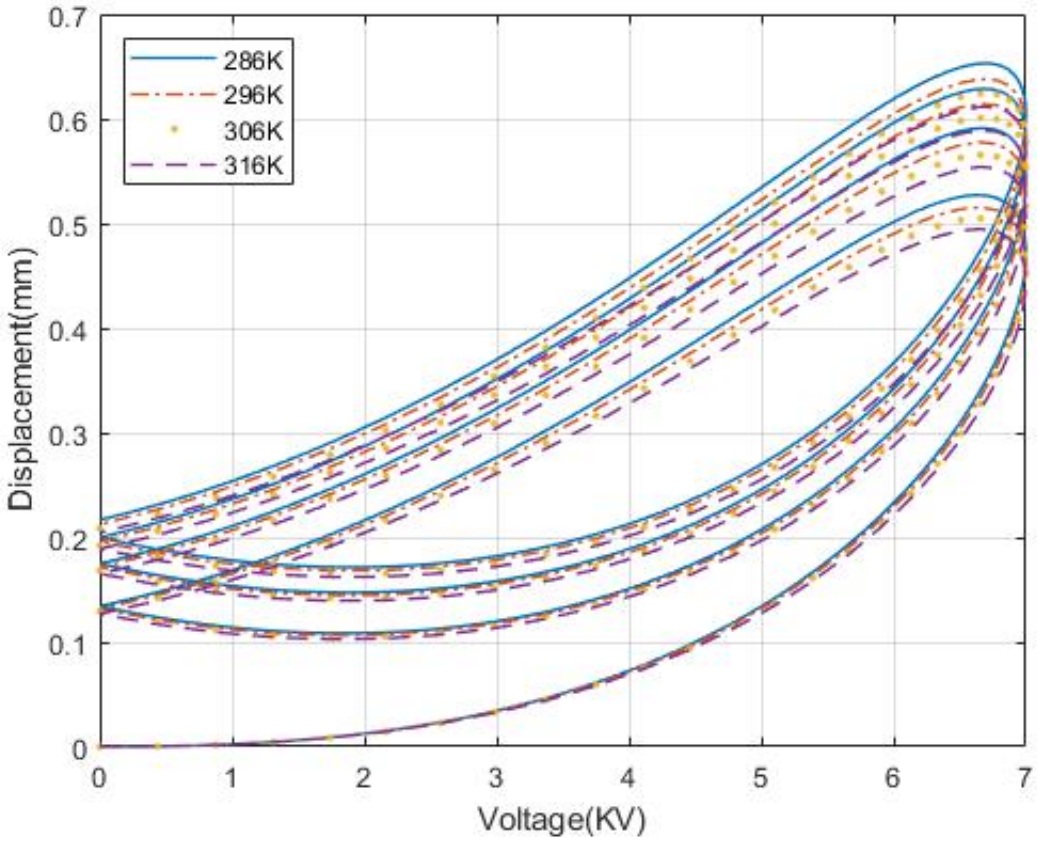

Figure 4.21: Displacement versus voltage for different temperatures.

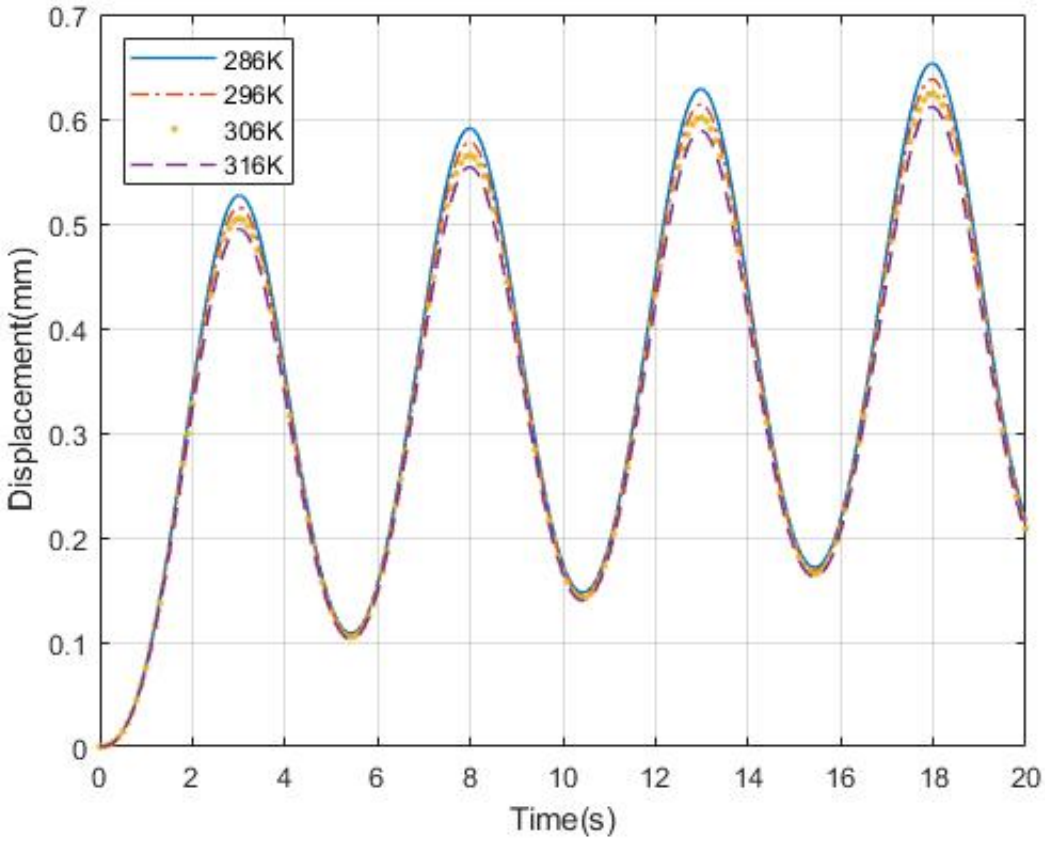

Figure 4.22: Displacement versus time for different temperatures.

Chapter 5

Conclusion and Future Work

5.1 Conclusion

This thesis focuses on building an electromechanical model of the Dielectric Elastomer Actuator subjected to different voltages, frequencies, and temperatures. Also, the model proposed considers the influence of the temperature and deformation on the permittivity of the DE. The DE material, such as the most popular material used for DEs VHB 4910, is commonly known for its strong nonlinear viscoelasticity, such as hysteresis, creep, and other viscoelastic behaviors. DEAs materials exhibit this kind of viscoelastic phenomenon. The viscoelastic behaviors of DEAs limit and worsen the efficiency of the controller performances, which will lead to oscillations or even instabilities. This thesis proposes an electromechanical coupled model of a rectangle dielectric elastomer actuator using the material VHB 4910. The electromechanical behaviour and nonlinear viscoelasticity of DEs such as the creep is considered in the presented model.

The model verification shows the electromechanical response of the DEA subjected to different patterns of voltages, frequencies, and temperatures. An experimental test with one set of voltage, frequency, and temperature was conducted to verify the proposed model, and the results agree with the simulation results to a great extent. In modeling the DEA, it is extremely important to understand the electromechanical response of DEAs, and take into account its viscoelastic behavior. Thus, this model can help in understanding the phenomena of DEAs. Furthermore, according to the experimental test; this model can be effective to predict the electromechanical response of DEAs,

which will improve the controller performance of such soft materials.

The main contributions are summarized as follows,

In Chapter (3):

- Virtual work principle is used to build the dynamic model of the DE.
- The proposed model is based on the free energy physical-based principle.
- The general Kelvin-Voigt model is applied to describe the viscolasticity of the DE.
- The Maxwell force together with the Electrostrictive force are considered in the presented model.
- In the proposed model, the permittivity of the DE is considered with the influence of temperature and deformation.

In Chapter (4):

- The Differential Evolution algorithm is used in this thesis to identify the model parameters of the DE.
- By comparing the experimental results and simulations results, we can show the effectiveness of the proposed model. Meanwhile, the model of the DE in this study can describe the dynamic characteristics of the DE very accurately.
- The simulations of the presented DE model subjected to different voltages, frequencies, and temperatures are provided. An experimental test with one set of voltage, frequency, and temperature was conducted, and agrees with the simulation results, which means the model is valid.

5.2 Future Work

The following are suggested future studies for the presented thesis:

- In this thesis, a dielectric elastomer actuator model has been proposed; however, the model only considers the creep characteristics of the DEA. As a future work, the model will be

developed to consider the hysteresis characteristics of the DEA since it experiences high hysteresis.

- The model presented is subjected to different patterns of voltages, frequencies, and temperatures. The simulations provided have been done to validate the model under these different patterns. However, the experimental test conducted was subjected to only one temperature $296K$ or 23°C, which is the room temperature. In future work, an adequate device will be implemented to measure the temperature accurately and to give the chance for conducting more experiments under a variety of temperatures.

- In Chapter (3), according to the experimental results of Jean-Mistral, the fitting parameters $a = 0.0533Fm^{-1}$, $b = 645.4224FKm^{-1}$, and $c = 3.1834Fm^{-1}$ were used in the model. Based on the experimental results done by Jean-Mistral, a very effective equation was built to describe the influence of temperature and deformation on the permittivity of the DE. As a future work, an applicable device to measure the permittivity of the DE will be used to directly test the value of the DE's permittivity, which will lead to building a more effective equation to include more parameters, adding more accuracy, and reaching a better conclusion.

- Even though the model of the DE built in this thesis can effectively describe the dynamic characteristics of the DE, the presented model is complicated. This means that the model may not be very applicable in the control of the DE directly. In future work, based on the proposed model in this study; we plan to build a Phenomenological model of the DE with a Rectangle Shape to meet the demands of the engineering field.

References

Ahmadi, S., Gooyers, M., Soleimani, M., & Menon, C. (2013). Fabrication and electromechanical examination of a spherical dielectric elastomer actuator. *Smart Materials and Structures*, *22*(11), 115004.

Bauer, S., Bauer-Gogonea, S., Graz, I., Kaltenbrunner, M., Keplinger, C., & Schwödiauer, R. (2014). 25th anniversary article: a soft future: from robots and sensor skin to energy harvesters. *Advanced Materials*, *26*(1), 149–162.

Biddiss, E., & Chau, T. (2008). Dielectric elastomers as actuators for upper limb prosthetics: Challenges and opportunities. *Medical Engineering and Physics*, *30*(4), 403–418.

Bilgili, E., Bernstein, B., & Arastoopour, H. (2001). Inhomogeneous shearing deformation of a rubber-like slab within the context of finite thermoelasticity with entropic origin for the stress. *International Journal of Non-linear Mechanics*, *36*(6), 887–900.

Brochu, P., & Pei, Q. (2010). Advances in dielectric elastomers for actuators and artificial muscles. *Macromolecular Rapid Communications*, *31*(1), 10–36.

Carpi, F., & De Rossi, D. (2005). Eyeball pseudo-muscular actuators for an android face. In *Smart structures and materials 2005: Electroactive polymer actuators and devices (eapad)* (Vol. 5759, pp. 16–22).

Carpi, F., De Rossi, D., Kornbluh, R., Pelrine, R. E., & Sommer-Larsen, P. (2011). *Dielectric elastomers as electromechanical transducers: Fundamentals, materials, devices, models and applications of an emerging electroactive polymer technology*. Elsevier.

Carpi, F., Frediani, G., & De Rossi, D. (2011). Opportunities of hydrostatically coupled dielectric elastomer actuators for haptic interfaces. In *Electroactive polymer actuators and devices*

(eapad) 2011 (Vol. 7976, p. 797618).

Chen, S., Deng, L., He, Z., Li, E., & Li, G. (2016). Temperature effect on the performance of a dissipative dielectric elastomer generator with failure modes. *Smart Materials and Structures*, *25*(5), 055017.

Chiang Foo, C., Cai, S., Jin Adrian Koh, S., Bauer, S., & Suo, Z. (2012). Model of dissipative dielectric elastomers. *Journal of Applied Physics*, *111*(3), 034102.

DuRant, H., & You, J. (2014). *Humans need not apply.* American Association for the Advancement of Science.

Eckerle, J., Stanford, S., Marlow, J., Schmidt, R., Oh, S., Low, T., & Shastri, S. V. (2001). Biologically inspired hexapedal robot using field-effect electroactive elastomer artificial muscles. In *Smart structures and materials 2001: Industrial and commercial applications of smart structures technologies* (Vol. 4332, pp. 269–281).

Feng, C., Yu, L., & Zhang, W. (2014). Dynamic analysis of a dielectric elastomer-based microbeam resonator with large vibration amplitude. *International Journal of Non-Linear Mechanics*, *65*, 63–68.

Gaskell, D. R., & Laughlin, D. E. (2017). *Introduction to the thermodynamics of materials*. CRC Press.

Gent, A. (1996). A new constitutive relation for rubber. *Rubber Chemistry and Technology*, *69*(1), 59–61.

Giousouf, M., & Kovacs, G. (2013). Dielectric elastomer actuators used for pneumatic valve technology. *Smart Materials and Structures*, *22*(10), 104010.

Godaba, H., Foo, C. C., Zhang, Z. Q., Khoo, B. C., & Zhu, J. (2014). Giant voltage-induced deformation of a dielectric elastomer under a constant pressure. *Applied Physics Letters*, *105*(11), 112901.

Godaba, H., Li, J., Wang, Y., & Zhu, J. (2016). A soft jellyfish robot driven by a dielectric elastomer actuator. *IEEE Robotics and Automation Letters*, *1*(2), 624–631.

Goulbourne, N., Mockensturm, E., & Frecker, M. (2005). A nonlinear model for dielectric elastomer membranes. *Journal of Applied Mechanics*, *72*(6), 899–906.

Goulbourne, N. C., Frecker, M. I., & Mockensturm, E. (2004). Electro-elastic modeling of a

dielectric elastomer diaphragm for a prosthetic blood pump. In *Smart structures and materials 2004: Electroactive polymer actuators and devices (eapad)* (Vol. 5385, pp. 122–134).

Gu, G.-Y., Zhu, J., Zhu, L.-M., & Zhu, X. (2017). A survey on dielectric elastomer actuators for soft robots. *Bioinspiration and Biomimetics*, *12*(1), 011003.

Heim, J. R., Polyakov, I., Zarrabi, A., & Hui, O. (2009, February 17). *Electroactive polymer transducers biased for increased output.* Google Patents. (US Patent 7,492,076)

Heydt, R., Kornbluh, R., Eckerle, J., & Pelrine, R. (2006). Sound radiation properties of dielectric elastomer electroactive polymer loudspeakers. In *Smart structures and materials 2006: Electroactive polymer actuators and devices (eapad)* (Vol. 6168, p. 61681M).

Hong, W. (2011). Modeling viscoelastic dielectrics. *Journal of the Mechanics and Physics of Solids*, *59*(3), 637–650.

Hong, W., Zhao, X., & Suo, Z. (2010). Large deformation and electrochemistry of polyelectrolyte gels. *Journal of the Mechanics and Physics of Solids*, *58*(4), 558–577.

Iskandarani, Y., & Karimi, H. R. (2012). Sensing capabilities based on dielectric electro active polymers feasibility and potential state-of-the-art application. *IEEE Sensors Journal*, *12*(8), 2616–2624.

Jean-Mistral, C., Sylvestre, A., Basrour, S., & Chaillout, J. (2010). Dielectric properties of polyacrylate thick films used in sensors and actuators. *Smart Materials and Structures*, *19*(7), 075019.

Jhong, Y.-Y., Huang, C.-M., Hsieh, C.-C., & Fu, C.-C. (2007). Improvement of viscoelastic effects of dielectric elastomer actuator and its application for valve devices. In *Electroactive polymer actuators and devices (eapad) 2007* (Vol. 6524, p. 65241Y).

Jiang, L., Betts, A., Kennedy, D., & Jerrams, S. (2016). Eliminating electromechanical instability in dielectric elastomers by employing pre-stretch. *Journal of Physics D: Applied Physics*, *49*(26), 265401.

Joglekar, M. (2014). An energy-based approach to extract the dynamic instability parameters of dielectric elastomer actuators. *Journal of Applied Mechanics*, *81*(9), 091010.

Jordan, G., McCarthy, D. N., Schlepple, N., Krissler, J., Schröder, H., & Kofod, G. (2011). Actuated micro-optical submount using a dielectric elastomer actuator. *IEEE/ASME Transactions on*

Mechatronics, *16*(1), 98–102.

Kaal, W., & Herold, S. (2011). Electroactive polymer actuators in dynamic applications. *IEEE/ASME Transactions on Mechatronics*, *16*(1), 24–32.

Keplinger, C., Kaltenbrunner, M., Arnold, N., & Bauer, S. (2010). Röntgen?s electrode-free elastomer actuators without electromechanical pull-in instability. *Proceedings of the National Academy of Sciences*, *107*(10), 4505–4510.

Kim, H., Park, J., Chuc, N. H., Choi, H., Nam, J., Lee, Y., ... Koo, J. (2007). Development of dielectric elastomer driven micro-optical zoom lens system. In *Electroactive polymer actuators and devices (eapad) 2007* (Vol. 6524, p. 65241V).

Kim, H. K., Hwang, S., Choi, H. R., Kim, H., Jeon, J., & Nam, J. (2001). Field-actuated behavior of polymers as dielectric material. In *Smart structures and materials 2001: Electroactive polymer actuators and devices* (Vol. 4329, pp. 491–499).

Kofod, G. (2001). *Dielectric elastomer actuators: Ph. d. thesis*. Risø National Laboratory.

Koh, S. J. A., Li, T., Zhou, J., Zhao, X., Hong, W., Zhu, J., & Suo, Z. (2011). Mechanisms of large actuation strain in dielectric elastomers. *Journal of Polymer Science Part B: Polymer Physics*, *49*(7), 504–515.

Kollosche, M., Kofod, G., Suo, Z., & Zhu, J. (2015). Temporal evolution and instability in a viscoelastic dielectric elastomer. *Journal of the Mechanics and Physics of Solids*, *76*, 47–64.

Kollosche, M., Zhu, J., Suo, Z., & Kofod, G. (2012). Complex interplay of nonlinear processes in dielectric elastomers. *Physical Review E*, *85*(5), 051801.

Lamba, N. K. (2017). *Polyurethanes in biomedical applications*. Routledge.

Laschi, C., & Cianchetti, M. (2014). Soft robotics: new perspectives for robot bodyware and control. *Frontiers in Bioengineering and Biotechnology*, *2*, 3.

Lau, G.-K., Lim, H.-T., Teo, J.-Y., & Chin, Y.-W. (2014). Lightweight mechanical amplifiers for rolled dielectric elastomer actuators and their integration with bio-inspired wing flappers. *Smart Materials and Structures*, *23*(2), 025021.

Lee, H. S., Phung, H., Lee, D.-H., Kim, U. K., Nguyen, C. T., Moon, H., ... others (2014). Design analysis and fabrication of arrayed tactile display based on dielectric elastomer actuator. *Sensors and Actuators A: Physical*, *205*, 191–198.

Li, T., Qu, S., & Yang, W. (2012). Electromechanical and dynamic analyses of tunable dielectric elastomer resonator. *International Journal of Solids and Structures*, *49*(26), 3754–3761.

Liu, L., Liu, Y., Li, B., Yang, K., Li, T., & Leng, J. (2011). Thermo-electro-mechanical instability of dielectric elastomers. *Smart Materials and Structures*, *20*(7), 075004.

Liu, L., Sun, W., Sheng, J., Chang, L., Li, D., & Chen, H. (2015). Effect of temperature on the electromechanical actuation of viscoelastic dielectric elastomers. *EPL (Europhysics Letters)*, *112*(2), 27006.

Liu, Y., Liu, L., Zhang, Z., & Leng, J. (2009). Dielectric elastomer film actuators: characterization, experiment and analysis. *Smart Materials and Structures*, *18*(9), 095024.

Maffli, L., Rosset, S., & Shea, H. (2013). Zipping dielectric elastomer actuators: characterization, design and modeling. *Smart Materials and Structures*, *22*(10), 104013.

Majidi, C. (2014). Soft robotics: a perspective current trends and prospects for the future. *Soft Robotics*, *1*(1), 5–11.

Marvel, J. A., Falco, J., & Marstio, I. (2015). Characterizing task-based human–robot collaboration safety in manufacturing. *IEEE Transactions on Systems, Man, and Cybernetics: Systems*, *45*(2), 260–275.

Mazzolai, B., Margheri, L., Cianchetti, M., Dario, P., & Laschi, C. (2012). Soft-robotic arm inspired by the octopus: Ii. from artificial requirements to innovative technological solutions. *Bioinspiration and Biomimetics*, *7*(2), 025005.

Michel, S., Zhang, X. Q., Wissler, M., Löwe, C., & Kovacs, G. (2010). A comparison between silicone and acrylic elastomers as dielectric materials in electroactive polymer actuators. *Polymer International*, *59*(3), 391–399.

Molberg, M., Leterrier, Y., Plummer, C. J., Walder, C., Löwe, C., Opris, D. M., … Månson, J.-A. E. (2009). Frequency dependent dielectric and mechanical behavior of elastomers for actuator applications. *Journal of Applied Physics*, *106*(5), 054112.

Mooney, M. (1940). A theory of large elastic deformation. *Journal of Applied Physics*, *11*(9), 582–592.

Ogden, R. W. (1972). Large deformation isotropic elasticity–on the correlation of theory and

experiment for incompressible rubberlike solids. *Proc. R. Soc. Lond. A*, *326*(1567), 565–584.

Park, H. S., & Nguyen, T. D. (2013). Viscoelastic effects on electromechanical instabilities in dielectric elastomers. *Soft Matter*, *9*(4), 1031–1042.

Patra, K., & Sahu, R. K. (2015). A visco-hyperelastic approach to modelling rate-dependent large deformation of a dielectric acrylic elastomer. *International Journal of Mechanics and Materials in Design*, *11*(1), 79–90.

Pei, Q., Rosenthal, M., Stanford, S., Prahlad, H., & Pelrine, R. (2004). Multiple-degrees-of-freedom electroelastomer roll actuators. *Smart Materials and Structures*, *13*(5), N86.

Pelrine, R., Kornbluh, R., Pei, Q., & Joseph, J. (2000). High-speed electrically actuated elastomers with strain greater than 100%. *Science*, *287*(5454), 836–839.

Pelrine, R., Kornbluh, R. D., Pei, Q., Stanford, S., Oh, S., Eckerle, J., ... Meijer, K. (2002). Dielectric elastomer artificial muscle actuators: toward biomimetic motion. In *Smart structures and materials 2002: Electroactive polymer actuators and devices (eapad)* (Vol. 4695, pp. 126–138).

Pelrine, R. E., Kornbluh, R. D., & Joseph, J. P. (1998). Electrostriction of polymer dielectrics with compliant electrodes as a means of actuation. *Sensors and Actuators A: Physical*, *64*(1), 77–85.

Plante, J.-S., & Dubowsky, S. (2006). Large-scale failure modes of dielectric elastomer actuators. *International Journal of Solids and Structures*, *43*(25-26), 7727–7751.

Plante, J.-S., & Dubowsky, S. (2007). On the performance mechanisms of dielectric elastomer actuators. *Sensors and Actuators A: Physical*, *137*(1), 96–109.

Rizzello, G., Naso, D., York, A., & Seelecke, S. (2015). Modeling, identification, and control of a dielectric electro-active polymer positioning system. *IEEE Transactions on Control Systems Technology*, *23*(2), 632–643.

Robinson, G., & Davies, J. B. C. (1999). Continuum robots-a state of the art. *Robotics and automation, 1999. Proceedings. 1999 IEEE International Conference on*, *(Vol. 4*, pp. 2849–2854).

Rosset, S., & Shea, H. R. (2013). Flexible and stretchable electrodes for dielectric elastomer

actuators. *Applied Physics A*, *110*(2), 281–307.

Rus, D., & Tolley, M. T. (2015). Design, fabrication and control of soft robots. *Nature*, *521*(7553), 467.

Sahu, R., Patra, K., & Szpunar, J. (2015). Experimental study and numerical modelling of creep and stress relaxation of dielectric elastomers. *Strain*, *51*(1), 43–54.

Sarban, R., Lassen, B., & Willatzen, M. (2012). Dynamic electromechanical modeling of dielectric elastomer actuators with metallic electrodes. *IEEE/ASME Transactions on Mechatronics*, *17*(5), 960–967.

Sheng, J., Chen, H., & Li, B. (2011). Effect of temperature on the stability of dielectric elastomers. *Journal of Physics D: Applied Physics*, *44*(36), 365406.

Sheng, J., Chen, H., Li, B., & Chang, L. (2013). Temperature dependence of the dielectric constant of acrylic dielectric elastomer. *Applied Physics A*, *110*(2), 511–515.

Sheng, J., Chen, H., Li, B., & Wang, Y. (2014). Nonlinear dynamic characteristics of a dielectric elastomer membrane undergoing in-plane deformation. *Smart Materials and Structures*, *23*(4), 045010.

Shepherd, R. F., Ilievski, F., Choi, W., Morin, S. A., Stokes, A. A., Mazzeo, A. D., ... Whitesides, G. M. (2011). Multigait soft robot. *Proceedings of the National Academy of Sciences*, *108*(51), 20400–20403.

Shintake, J., Rosset, S., Schubert, B. E., Floreano, D., & Shea, H. R. (2015). A foldable antagonistic actuator. *IEEE/ASME Transactions on Mechatronics*, *20*(5), 1997–2008.

Sommer-Larsen, P., Kofod, G., Shridhar, M., Benslimane, M., & Gravesen, P. (2002). Performance of dielectric elastomer actuators and materials. In *Smart structures and materials 2002: Electroactive polymer actuators and devices (eapad)* (Vol. 4695, pp. 158–167).

Son, S.-i., Pugal, D., Hwang, T., Choi, H. R., Koo, J. C., Lee, Y., ... Nam, J.-D. (2012). Electromechanically driven variable-focus lens based on transparent dielectric elastomer. *Applied Optics*, *51*(15), 2987–2996.

Storn, R., & Price, K. (1995). Differential evolution-a simple and efficient adaptive scheme for global optimization over continuous spaces [r]. *Berkeley: ICSI*.

Sugimoto, T., Ando, A., Ono, K., Morita, Y., Hosoda, K., Ishii, D., & Nakamura, K. (2013). A

lightweight push-pull acoustic transducer composed of a pair of dielectric elastomer films. *The Journal of the Acoustical Society of America*, *134*(5), EL432–EL437.

Suo, Z. (2010). Theory of dielectric elastomers. *Acta Mechanica Solida Sinica*, *23*(6), 549–578.

Vertechy, R., Fontana, M., Papini, G. R., & Bergamasco, M. (2013). Oscillating-water-column wave-energy-converter based on dielectric elastomer generator. In *Electroactive polymer actuators and devices (eapad) 2013* (Vol. 8687, p. 86870I).

Vu-Cong, T., Jean-Mistral, C., & Sylvestre, A. (2013). New operating limits for applications with electroactive elastomer: Effect of the drift of the dielectric permittivity and the electrical breakdown. In *Electroactive polymer actuators and devices (eapad) 2013* (Vol. 8687, p. 86871S).

Wissler, M., & Mazza, E. (2005). Modeling of a pre-strained circular actuator made of dielectric elastomers. *Sensors and Actuators A: Physical*, *120*(1), 184–192.

Xu, B.-X., Mueller, R., Theis, A., Klassen, M., & Gross, D. (2012). Dynamic analysis of dielectric elastomer actuators. *Applied Physics Letters*, *100*(11), 112903.

Yeoh, O. (1990). Characterization of elastic properties of carbon-black-filled rubber vulcanizates. *Rubber Chemistry and Technology*, *63*(5), 792–805.

Zhang, C., Chen, H., Li, B., Wang, Y., Liu, L., & Li, D. (2015). Investigation on static and dynamic performance of a hinge configuration with integrated dielectric elastomers. *Journal of Applied Polymer Science*, *132*(11).

Zhao, X. (2014). Multi-scale multi-mechanism design of tough hydrogels: building dissipation into stretchy networks. *Soft Matter*, *10*(5), 672–687.

Zhao, X., Hong, W., & Suo, Z. (2007). Electromechanical hysteresis and coexistent states in dielectric elastomers. *Physical Review B*, *76*(13), 134113.

Zhao, X., & Suo, Z. (2007). Method to analyze electromechanical stability of dielectric elastomers. *Applied Physics Letters*, *91*(6), 061921.

Zhao, X., & Suo, Z. (2008). Electrostriction in elastic dielectrics undergoing large deformation. *Journal of Applied Physics*, *104*(12), 123530.

Zhao, X., & Suo, Z. (2009). Electromechanical instability in semicrystalline polymers. *Applied Physics Letters*, *95*(3), 031904.

Zhao, X., & Suo, Z. (2010). Theory of dielectric elastomers capable of giant deformation of actuation. *Physical Review Letters*, *104*(17), 178302.

Zhao, X., & Wang, Q. (2014). Harnessing large deformation and instabilities of soft dielectrics: Theory, experiment, and application. *Applied Physics Reviews*, *1*(2), 021304.

Zhou, J., Jiang, L., & Khayat, R. E. (2015). Investigation on the performance of a viscoelastic dielectric elastomer membrane generator. *Soft Matter*, *11*(15), 2983–2992.

Zhu, J., Cai, S., & Suo, Z. (2010). Resonant behavior of a membrane of a dielectric elastomer. *International Journal of Solids and Structures*, *47*(24), 3254–3262.

Zhu, J., Kollosche, M., Lu, T., Kofod, G., & Suo, Z. (2012). Two types of transitions to wrinkles in dielectric elastomers. *Soft Matter*, *8*(34), 8840–8846.